AMERICAN UNIVERSITY OF BEIRUT

EEG Artifact Removal for Ambulatory Epileptic Seizure Prediction Applications

by

Md Shafiqul Islam

Beirut, Lebanon
July 2017

AMERICAN UNIVERSITY OF BEIRUT

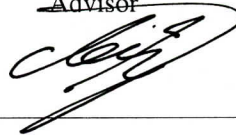# EEG Artifact Removal for Ambulatory Epileptic Seizure Prediction Applications

by
Md Shafiqul Islam

Approved by:

Dr. Zaher Dawy, Professor, AUB   Advisor

Electrical and Computer Engineering
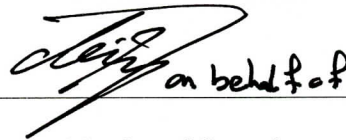
Dr. Hazem Hajj, Associate Professor, AUB   Member of Committee

Electrical and Computer Engineering   on behalf of

Dr. Ahmad El-Hajj, Assistant Professor, BAU   Member of Committee

Electrical and Computer Engineering

Date of thesis defense: July 27, 2017

AMERICAN UNIVERSITY OF BEIRUT

THESIS, DISSERTATION, PROJECT
RELEASE FORM

Student Name: __ISLAM   MD SHAFIQUL   MD YUNUS__

               Last   First   Middle

☑ Master's Thesis   ◯ Master's Project   ◯ Doctoral Dissertation

☐   I authorize the American University of Beirut to: (a) reproduce hard or electronic copies of my thesis, dissertation, or project; (b) include such copies in the archives and digital repositories of the University; and (c) make freely available such copies to third parties for research or educational purposes.

☑   I authorize the American University of Beirut, to: (a) reproduce hard or electronic copies of it; (b) include such copies in the archives and digital repositories of the University; and (c) make freely available such copies to third parties for research or educational purposes after: **One** ___ year from the date of submission of my thesis, dissertation or project.
       Two ___ years from the date of submission of my thesis, dissertation or project.
       Three ✓_ years from the date of submission of my thesis, dissertation or project.

Shafiq   _02.08.2017_

    Signature   Date

Acknowledgements

Pursuing a graduate degree at AUB is a demanding and sometimes a lonely path for me. I still remember my first meeting with Dr. Dawy in his office and his inspiration. Before that meeting, things were not looking so smooth. I had no idea where my higher studies was heading and whether it was possible to finish given my circumstances. There was a gap in my studies as I was serving in an industry for about three years. Dr. Dawy gave me hope and made me realize that with determination and hard work, pursuing my dream was not an impossible task. Dr. Dawy is a great advisor with high caliber, who can uncover the hidden potential of a student. He always listened to me to understand what I really had issues with and guided me to a direction in which I could excel as he was well aware about my strength and weakness. I am indebted for his constant assistance, encouragement, guidance and the tremendous support and opportunities he provided throughout my graduate studies. Dr. Dawy not only put enormous amount of time and effort into directing this thesis work but he also helped in refining the ideas and confirming every aspect of research results to the tiniest level of detail. I am very lucky, as many of my friends said, to have Dr. Dawy as my adviser and many many thanks for all he has done for me.

I am also pleased to acknowledge the support of Dr. Hazem Hajj, my thesis committee member for his valuable input during thesis proposal presentation. Special heartiest thanks for Dr. Hajj for providing useful comments in the development of my thesis.

I am so grateful to my thesis committee member, Dr. Ahmad, for being friendly, caring, supportive and helpful in numerous ways. I got valuable and well organized suggestions not only for my research work but also for choosing graduate courses, making effective and balanced study plan during my staying at AUB. He was always ready with constructive feedback on my thesis progress. Also, Dr. Ahmad helped me sharpen my critical thinking and writing skills during write up of conference and journal paper.

Additionally, I would like to extend my thanks and appreciation to my colleague, Hussein Alawieh, of Neuro Research Group at AUB, for his outstanding help in im-

An Abstract of the Thesis of

Md Shafiqul Islam   for   Master of Engineering

Major: Electrical and Computer Engineering

Title: EEG Artifact Removal for Ambulatory Epileptic Seizure Prediction Applications

Electroencephalography (EEG) is considered a primary tool for monitoring the electrical activity of the brain. Recent advances in wearable sensing techniques allow continuous and mobile monitoring of EEG signals during daily life activities. However, such method of EEG recording is prone to different sources of artifacts: eye-movement, electrode movement, muscle contraction, line noise, head movement and others. Among these sources, motion-related artifacts are a major challenge for clean EEG data acquisition. The significant effect of motion artifacts is evident in two main aspects. First, they overlap with all EEG frequency bands. Second, they spread over the entire scalp affecting all sensing electrodes. For some neuro applications, such as epileptic seizure detection and prediction, high quality EEG signals are required to accurately depict the electrical activity of the brain and thus track seizure markers for correct classification. The main focus of this thesis work is to record EEG data with defined motion artifacts in a controlled lab environment, to utilize various algorithmic methods for the effective elimination of motion artifacts, to assess the performance of the adopted artifact removal technique using statistical measures, and to employ the latter technique in the application of seizure detection and prediction. The adopted approach for artifact removal is based on applying independent component analysis (ICA) as a blind source separation technique for removing mobility artifacts from EEG data. The quality of the reconstructed EEG signals is assessed first using various statistical measures and then through investigating the seizure-prediction and seizure-detection capabilities of the reconstructed signals as opposed to the capabilities of the original noise-free signals. For detection and prediction purposes, the EEG signals are analyzed by extracting distinctive features using an N-gram based algorithm. These features are used to train a predictive model, which is in turn used it to classify EEG segments based on the random forest classifier. In the testing phase, the reconstruction of seizure-related data (namely, ictal data) by ICA was validated using time, frequency, and statistical signal similarity measures. In addition, the effect of

mobility artifacts on seizure detection and prediction is analyzed extensively on standard EEG recordings from the Freiburg EEG database, to which simulated mobility noise is added. The testing results showed that the prediction and detection accuracies decreased upon the addition of mobility noise then increased after implementing ICA for artifact separation. This proves that ICA was capable of separating the recorded and simulated mobility artifacts from EEG data while preserving signal trends and seizure-related features what consequently led to prediction and detection accuracies that are comparable to the noise-free case.

Contents

List of Figures

List of Tables

Chapter 1

Introduction

Electroencephalography (EEG) is an electrophysiological monitoring method to record the electrical activity of the brain. It is typically noninvasive, with the electrodes placed on the scalp. Invasive electrodes are mainly used in specific surgical cases. EEG measures voltage fluctuations resulting from ionic current circulating the neurons of the brain [1]. In clinical contexts, EEG refers to the recording of the brains spontaneous electrical activity over a period of time, as recorded from multiple electrodes placed on the scalp. Diagnostic applications generally focus on the spectral content of EEG, that is, the type of neural oscillations (popularly known as brain waves) that can be observed in EEG signals. EEG is most often used to diagnose epilepsy, which causes abnormalities in EEG readings [2]. It is also used to diagnose sleep disorders, coma, encephalopathy, and brain death. EEG used to be a first-line method of diagnosis for tumors, stroke and other focal brain disorders [3] but this use has decreased with the advent of high-resolution anatomical imaging techniques such as magnetic resonance imaging (MRI) and computed tomography (CT). Despite limited spatial resolution, EEG continues to be a valuable tool for research and diagnosis, especially for applications that require millisecond-range temporal resolution what is not possible with CT or MRI.

Traditional EEG systems require the subject to stay still in the hospital while brain signals are being acquired. Engineering advancements in terms of sensor design, low energy wireless transmission and frugal processing hardware have led to the development of new wireless headsets which are more suitable for mobile recording [4]. However, such continuous mobile recording of EEG is prone to motion-related artifacts, which potentially originate from cable sway or movements of the recording electrodes in relation relative to the scalp [5]. EEG artifacts from cyclical motions such as walking are influenced by movement speed and can have a power spectral density covering a relatively wide range of low and high frequencies [5]. This imposes a major challenge on current signal processing techniques and limits their ability to handle such type of motion artifacts in mobile EEG recording.

EEG has been extensively used in epilepsy monitoring units (EMUs) for long continuous recording of patients brain activities that is later used for research and diagnostic purposes. Epilepsy is one of the most common neurological disorders, second only to stroke, with a prevalence of 0.6-0.8% of the worlds population. Epilepsy can significantly impact a patients career choice, lifestyle, and recreational activities (e.g. bathing and swimming alone). Even simple daily life tasks like using a knife or driving a car could present a serious threat on an epilepsy patient who cant predict seizure onsets. These potential harmful consequences of epilepsy and the fact that not all patients respond to treatment gave an incentive for developing a continuous monitoring system with a predictive capability that gives alarms of incoming seizure episode ahead of time so that the patient can take necessary precautions. Not only the prediction but also the detection of epileptic seizures is of great importance. Detection can be extremely useful in extensive care units or for coma patients in order to apply targeted stimulation that mitigates the seizures effect. For proper functioning of an epilepsy monitoring system, a systematic approach is required for recognition, source identification, and elimination of motion artifact to reduce the chance of inaccurate diagnosis and limit the potential for adverse clinical consequences. Accurate ambulatory detection and prediction of epileptic seizures require clean and artifact-free EEG signals. However, such a requirement is considered a major challenge because EEG signals are vulnerable to various forms of artifacts caused by muscle activity and body movement [6]. Thus, customized signal processing techniques are required to remove these motion related artifacts and to ensure high quality EEG signals.

Motion artifacts due to body movements share the same frequency spectra with EEG (up to 50Hz) and have amplitude that is an order of magnitude larger than the clean brain-related EEG signals [7]. Some studies have suggested various methods to clean EEG signals from motion artifacts. Most of these studies have been limited to highly-controlled laboratory environments [8]. Filtering is the most widely used signal processing technique to remove artifacts. In [9], several approaches such as Wiener, adaptive, and Kalman filtering techniques have been used to remove different types of artifacts from EEG. However, one major limitation of these filtering approaches is their dependency upon a measured or reliably estimated reference for proper operation. Alternatively, blind source separation (BSS) techniques have been proposed to estimate brain signals from noisy observations, without the need for a reference waveform. Among the different approaches of BSS, independent component analysis (ICA) is the most frequently used technique for the removal of artifacts from EEG [10]. By applying ICA techniques, it has been shown that artifacts and epilepsy related brain signals can be successfully separated as independent components [11].

This thesis work deals with the mobility artifactual EEG data acquisition followed by a thorough analysis of different types of motion artifacts and an investigation of various artifact removal techniques. The efficiency of these approaches has been assessed in the scope of seizure detection and prediction application based on artifact-colored

EEG signals. The resulting accuracies and sensitivities of the algorithms would then be used as a performance metric to estimate the quality of artifact removal. In particular, high levels of accuracy and sensitivity would reflect the fact that the distinctive seizure markers have been correctly identified in the EEG signals and that the artifact related components hiding these markers have been successfully removed. The key contributions of this thesis work are highlighted below:

1. Analyzing EEG artifacts resulting from physical mobility using an experimental approach. This entails acquiring EEG data with recorded motion artifacts using wearable sensing EEG headset (This work is specifically concerned with variable speed walking artifacts).

2. Studying the performance of different artifact removal techniques. ICA was then adapted to separate mobility artifacts, and its parameters were optimized in this context.

3. Investigating the impact of mobility artifacts and the effectiveness of the artifact removal techniques on epileptic seizure prediction and detection. Recorded mobility artifacts as well as simulated mobility noise were added to EEG data from the Freiburg database. Distinctive features were extracted using the N-Gram approach and the random forest machine learning algorithm was later used for classification in prediction and detection of seizures.

The thesis is organized as follows. Chapter 2 includes a detailed review of various related artifact removal techniques as well as epilepsy prediction and detection methods available in the literature. Chapter 3 presents the setup for mobile EEG data acquisition with details analysis. Chapter 4 describes the proposed methodology for mobility artifact removal with evaluation of effective reconstruction. Chapter 5 includes assessment of the impact of those mobility artifacts on epilepsy prediction and detection. Finally, Chapter 6 concludes the thesis.

Chapter 2

Literature Survey

The objective of this literature survey is to investigate previous work related to the thesis topic. It starts with a brief introduction on EEG artifacts and their classification. Then, it discusses the mobility artifact removal techniques available in the literature with a comparison of different approaches. After that, it presents different epilepsy prediction and detection techniques with emphasis on the N-gram based approach, and it includes a brief overview about the Freiburg epileptic database. Finally, this chapter presents a brief summary of the major relevant finding in literature with their limitations in the scope of the presented work.

2.1 EEG Artifacts

Artifacts can be defined as unwanted components overlapping with the signal of interest [12]. Usually, the characteristics of artifacts differ from those of the signals under study. In the frequency domain, artifacts are known to occupy a defined frequency range. They correspond to discrete frequencies and their harmonics. They are also limited to a certain time range defined by the duration of the events that caused them (e.g., the case of eye blinks) and to a subspace of the signal space. Also they are characterized by particular temporal patterns such as exponential decay. An important characteristic of artifacts is that they can be assumed to be sufficiently independent of the observed signals.

2.1.1 Artifact Types

Various types of artifacts associated with EEG recordings are briefly described in the following subsequent sections.

Ocular Artifact

The ocular artifact (OA) is generated upon eye movements and is normally strong enough to be recorded along with the EEG signals. The amplitude of the blinking

artifact is generally much larger than that of the background EEG activity. OA occurs within the range of 0-16Hz.

Muscle Artifacts

The muscle artifact (EMG) is caused by the contraction of muscles. This artifact is commonly present during the recordings of patients who are awake since it appears when the patient swallows, talks, walks, etc.. EMG presents a wide spectral distribution, thus it perturbs all classical EEG frequency bands; in particular it considerably overlaps with beta activity in the 15-30 Hz range but can also be as low as 2 Hz what makes the widely used alpha band also vulnerable to muscle artifacts.

Artifacts due to Cardiac Activity

Cardiac activity or electrocardiogram (ECG) measures the electrical activity of the heart. The amplitude of the cardiac activity on the scalp is usually low. ECG has a very characteristic repetitive and regular pattern, which may sometimes be mistaken for epileptiform activity when the ECG is barely visible in EEG recordings.

physiological artifacts

Other physiological artifacts such as perspiration artifacts are manifested as slow waves caused by shifts in the electrical baseline of certain electrodes. To a smaller extent, the sympathetic skin response, which also consists of slow waves and is an autonomic response produced by sweat glands and skin potentials, may be present in EEG recordings.

Non-physiological artifacts

There are also non-physiological artifacts which may interfere EEG. The electrical and wireless interference of external equipment such as power lines, wireless devices, cables, computers and high-frequency signal generators in addition to internal electrical noise interference caused by electrodes, electrode positions, caps, cables and amplifiers.

2.2   Artifacts Removal

This section gives a comprehensive overview of techniques that can be used for the removal of artifacts from EEG.

2.2.1 Linear Regression

Regression algorithms were arguably the most frequently used EEG artifact correction techniques up to the mid-1990s, especially for ocular interferences. Linear regression assumes that each EEG channel is the sum of the non- noisy source signal and a fraction of the artifact that is available through a reference channel. The goal of regression is to estimate the optimal value for the factor that represents such a propagation fraction. In multiple linear regressions the measured signal of each electrode is influenced by more than one (fraction of the) reference wave forms (for instance: vertical, horizontal and radial ocular artifacts). Regression methods had been replaced by more sophisticated algorithms primarily because the former need one or more reference channels a disadvantage that mainly limits their applicability to removing EOG and ECG artifacts [13].

2.2.2 Filtering

Generally, filtering is not suitable for canceling artifacts from EEG recordings because of the overlapping frequency spectrum corresponding to the artifacts and the signal of interest. However, various artifact removal techniques based on filtering, as described in this section, try to adapt filter parameters to minimize the mean square error between the estimated and the desired EEG signals. What follows briefly highlights the main filtering techniques employed in the removal of artifacts from EEG.

Adaptive filtering

In the scope of artifact removal, adaptive filtering works based on the assumption that a correlation between the brain signals and the artifacts. A noisy signal is estimated from a noisy reference signal and subtracted from the acquired EEG [14]. The main challenge here is the selection of the noisy reference signal for proper functioning of the algorithm. For instance, EOG signals can be used as a reference for the removal of eye movement or blinking artifacts [15] and similarly EMG signals can be used for the removal of muscle artifacts [16]. Adaptive filters iteratively adjust a vector of weights based on an optimization algorithm. These weights model the degree of contamination of EEG with artifacts. The most prevalent family of algorithms is based on the least mean squares method, which is linear in complexity and convergence. Another well-known family is based on the recursive least squares (RLS) method, which is quadratic in complexity and convergence [14].

Wiener filtering

Wiener filtering is another parametric technique, based on a statistical approach, which produces a linear time-invariant filter to minimize the mean square error between the desired signal and its estimate [17]. The minimization is done using an estimation of

the power spectral densities of the signal and the artifacts; hence it does not need a reference waveform. The disadvantages are the need for calibration prior to usage and the inability to run in real time. However, when properly calibrated, it can achieve a better signal to noise ratio (SNR) compared to adaptive filters [17].

Bayes filtering

Bayes filtering is a probabilistic system estimation method that starts from noisy observations [9]. These filters overcome some of the limitations of the aforementioned techniques as they are capable of working without a reference signal and can operate in real time. Bayes filters are not directly implementable due to their complexity; instead, they are approximated through Kalman filters and particle filters- the former has been used for nonlinear EEG artifact removal in [18]. Bayes filters first estimate the state at any given time instance and then obtain a feedback in the form of noisy measurements, which is used to predict a new a priori estimate [18].

2.2.3 Blind Source Separation

Blind source separation, also known as blind signal separation, is the separation of a set of source signals from a set of mixed signals, without the aid of information (or with very little information) about the source signals or the mixing process. Among the BSS techniques, principal component analysis (PCA) and independent component analysis (ICA) are two well-known algorithms utilized in the literature for artifact separation.

Principle Component Analysis

PCA uses an orthogonal transformation to convert the observations of possibly correlated variables into values of linearly uncorrelated variables called principal components, less than or equal in number to the original variables. The greatest problem with PCA is that the assumption of Orthogonality between neural activity and typical physiological artifacts does not generally hold. In fact, it has been demonstrated that PCA is unable to separate some artifactual components from brain signals, especially when they have similar amplitudes [19].

Independent component analysis

Independent component analysis (ICA) is a computational method for separating a multivariate signal into additive subcomponents. This is done by assuming that the subcomponents are non-Gaussian signals and that they are statistically independent from each other. Independence is a stronger assumption than uncorrelateness. In contrast to the possibly incorrect assumptions of PCA, it is the case that artifacts and brain activity are usually sufficiently independent, which explains the effectiveness of ICA for artifact removal [20].

2.2.4 Source Decomposition

Alternatively, the problem of finding artifact-free signals from observations can be tackled directly by decomposing each individual channel signal into a basic waveform that represents either the signal or the artifact, what allows removing the latter when present. Successful algorithms of this type are based on the fact that some sources (either signals or artifacts) can be represented by a single decomposition unit, such as an intrinsic mode function (IMF) for empirical mode decomposition, or by a certain wavelet basis for the wavelet transform.

Empirical mode decomposition [22] is a heuristic one-dimensional technique that aims at decomposing a signal into its basis functions, called intrinsic mode functions (IMFs), which are amplitude and frequency modulated zero mean components, plus a non-zero mean low degree polynomial remainder.

Wavelets are ideal for biomedical applications because of their versatility; they allow designing robust methods, and they have a finely tunable time frequency trade-off such that they can accommodate biomedical signals that generally combine features with good time or frequency localization [21].

2.2.5 Seminal Work on Motion Artifacts Removal

As mentioned earlier, obtaining a good quality EEG signal is crucial for the correct performance of any epilepsy related application. Motion artifacts are mainly related to the electrical activity on the body surface caused by the contraction of muscles. These artifacts are typical of patients who are awake and occur whenever the patient performs a muscular activity [17]. Shapes, trends, and amplitudes of the interference corresponding to motion related artifacts depend on the type of the involved muscle and its degree of contraction; hence, they are hard to stereotype [16].
Several properties of motion artifact are responsible for its adverse effects on the background EEG activity [23] what imposes great challenges relative to other types of artifacts [24]. Motion artifacts have a wide spectral distribution, thus they perturb all classical EEG frequency bands. In particular, their corresponding frequency spectrum considerably overlaps with beta band in the 15-30Hz range [25]. Their spectrum can also extend to as low as 2Hz [26], making the widely used alpha band also vulnerable to muscle artifacts [24]. Finally, motion artifacts are also associated with less repetitive trends as compared to other biological artifacts. Consequently, they are more difficult to characterize. This arises from the fact that these artifacts originate from the activity of spatially distributed, functionally independent muscle groups, with distinct topographic and spectral signatures [15].

The aforementioned properties of motion artifacts increase the complexity of the preprocessing stage required before the safe use of EEG signals. Several approaches were proposed in the literature to deal with motion artifacts. Table 2.1, outlines the most influential work done in motion artifact removal. In [27] eight healthy volunteers participated in an experiment for recording EEG signals while standing still, walking

Types of Motion	Algorithm used	Result
Treadmill Walking with a speed of 0.4-1.6 m/s	Infomax ICA	ICA and dipole fitting accurately localized 99% of the independent components in non-neural locations or lacked dipolar characteristics.
Head Movement	Two classifier 1. Decision Tree 2. HMM	Authors claim a substantial reduction in motion artifact.
Head Shaking, Nodding, Walking	CCA** and MLP* filtering	Recovery-82.4%
Walking in Real time	Kalman Filter	Restore contaminated EEG up to 93%
Real Time Walking and Running	Moving average and Wavelet decompose	This study showed that mechanical artifact can be minimized using the mentioned algorithm.

Table 2.1: Seminal work on motion artifacts removal

(0.8 and 1.25 m/s) and running (1.9 m/s) on a treadmill. Recorded data was decomposed using infomax ICA and after removing the noisy component, reconstructed EEG signals were reported with 99% accuracy. The work in [28] aimed to classify the head movement artifact using a data driven machine learning approach. Decision tree and Hidden Markov Model (HMM) classifiers were used and resulted in respective accuracies of 85% and 95%. A motion artifact reduction algorithm was proposed in [29] based on a multi-channel linear prediction filter(MLP). Canonical correlation analysis (CCA) was performed to detect artifacts what resulted in a substantial reduction of motion artifacts. Kalamn filter was used to estimate artifact template and EEG in the work of [30]. Then artifacts were subtracted from raw EEG signals and a 93% reconstruction was reported. In [31], motion artifactual EEG data was recorded from 9 subjects walking on a treadmill with a speed of 0.4 to 1.6 m/s. Moving average and wavelet decomposition were utilized to separate motion artifacts. This study in [31] claimed that motion artifacts cannot be fully removed from EEG.

2.3 Epileptic Seizures

A seizure is a sudden change in the normal electrical activity of the brain, which may produce a physical convulsion, minor physical signs, thought disturbances, or a combination of symptoms [32]. The symptoms that appear during a seizure depend on a variety of factors including: the location in which the irregular electrical activity takes place, the patients age, and the patients health condition. Seizure occurrences can be initiated by head wounds, brain tumors, lead poisoning and mal development

of the brain, genetic and infectious illnesses, and fevers. However, in nearly half of the cases, no clear cause can be tracked or identified. Seizures can be mainly divided into three categories:

- Absence seizures: these seizures disconnects a patient from the surrounding while he/she stare off vacantly for a moment until recovering a normal state without remembering what happened.

- Generalized tonic clonic seizures: these seizures begin with stiffening of the arms and legs followed by jerking motions of the limbs. Many individuals may fall from standing position while experiencing such seizures since generalized seizures may last for about five minutes.

- Partial seizure: unlike generalized seizures, these seizures affect only one side of the brain. Their symptoms depend on which area of the brain is affected. For example, if the motor area is affected, the patient may jerk fingers or move hands while if a sensory area is affected, the patient may hear sound or smell an odor that is not present.

2.3.1 Seizure Detection

Epileptic seizure detection refers to correctly identifying the seizure onset by distinguishing ictal periods from pre-ictal ones based on the variation in time, frequency and time-frequency domain features of the signals [33]. This detection provides useful data especially to personnel responsible for epilepsy monitoring units. The aim of seizure detection systems is to locate a seizure onset if present in the data. Most of the seizure detection algorithms involve the extraction of features to differentiate ictal from pre-ictal periods. This allows later classification of the EEG segments based on different learning techniques.

2.3.2 Seizure Prediction

Epileptic seizure prediction algorithms try to forecast the onset of a seizure ahead of time without a priori knowledge of the exact time of occurrence [34]. Seizure prediction methods can widely vary given the abundance of signal processing, mathematical, and statistical tools that could be applied to the problem of tracking pre-ictal changes throughout long stretches of EEG recordings. The performance of seizure prediction algorithms is usually assessed based on the sensitivity, which measures the proportion of correctly identified seizures among all seizure events and the false alarm rate, which measures the rate of falsely raised alarms.

2.3.3 Seminal Work on Seizure Detection and Prediction

Algorithms developed in this area mainly look at the variations of EEG signals across three dimensions: time variations, spectral (frequency) variations, and spatial variations (among different locations in the brain). Table 2.2 highlights the most influential work related to epileptic seizure prediction and detection.

Time domain features measure entities of the EEG signal that depend only on time. Classical and advanced signal analysis techniques are used to derive a wide range of time domain features capable of characterizing linear and non-linear behaviors of EEG signals. An n-gram based approach was adopted in [35] for extracting distinctive features from EEG data. The method uses a symbolic data analysis of EEG based on n-gram modeling, a probabilistic pattern recognition technique which identifies and predicts the occurrence of symbolic data sequences based on previous occurrences of these sequences. The variations of the number of occurrences of amplitude patterns in sequences of defined lengths give evidence of certain brain activity. The abrupt change in the electrical activity of the brain during a seizure would increase the variability of the EEG signal amplitudes and thus decrease the counts of previously recurrent and rhythmic amplitude patterns. Simulation results in [36] on the Freiburg dataset demonstrate high sensitivity values with relatively low false alarm rates. Frequency

Approach	Data Set	Feature	Classification Model	Result
Time Domain[6]	Freiburg, 623h iEEG, 87 Seizure, 21 Patients	Significant Pattern, N-Gram	Thresholding	93.81% Sensitivity, 6% false alarm
Frequency Domain [7]	European, 183 seizures, 3565h, 24 Patients	Sub-band Spectral Power	SVM	Sensitivity -75.8% False Alarm - 0.1/h
Time-Frequency [8]	15 Patients, iEEG, 24 months	Statistical, Energy	One-class SVM	97.1% Sensitivity 1.56% False alarm/h
Neuronal model [9]	7 Patients, 50 seizure	Time averaged Spiking rate	Thresholding 83-91%	Only 2 false alarm reported

Table 2.2: Seminal work on epileptic seizure detection and prediction

domain analysis looks at the spectral components of the EEG signals. Frequency domain features are derived from the spectral content of the EEG obtained through a transformation of the time-domain signal. The main spectral feature is the spectral power, often defined as the statistical estimate of the signal power in each frequency component and referred to as the power spectral density(PSD). The PSD has been extensively used in EEG analysis to identify and classify activities and states. The study in [37] presents an algorithm based on spectral power ratios. The authors trained and tested their learning models on long-term continuous datasets from 24 patients of the EPILEPSIAE database (183 ictal events in 3565 hours). Channels from 3 electrodes in the seizure onset area and 3 in remote areas were analyzed. Normalized spectral

powers of the EEG standard spectral bands (Delta, Theta, Alpha, Beta, and Gamma), were calculated for each channel over a five-second moving window. The authors used the ratio between normalized spectral powers as a feature to track pre-ictal changes. A feature selection routine along with a support vector machine classifier were used for building a machine learning model to classify events into inter-ictal events (not preceding a seizure onset) to pre-ictal events (preceding a seizure onset).

Finally, time-frequency analysis combines both time and frequency information into a single representation. This technique has proven to be a powerful tool for the analysis of non-stationary signals and have been used for seizure prediction. An example of such a study was performed in [38] where seizure prediction was assessed for 15 adult patient with drug resistant focal epilepsy.

As an alternative to a direct analysis of EEG characteristics, neural computation models were investigated to simulate the behavior of the neuronal activity by mathematical and computational processes in an attempt to describe the individual or collective neural mechanisms and obtain a mathematical model of the EEG activity for different brain states. An example of an epilepsy related study can be found in [39]. Another study in [40] presents a seizure prediction algorithm based on a computational model where features are estimated from the model fitted to EEG data. After pre-processing the data through filtering, the model was fitted to the frequency spectrum of intracranial EEG segments using a Bayesian inference method. The method was evaluated using the Freiburg database. The system achieved an average sensitivity of 87.1% and 92.6% and an average false prediction rate of 0.15 and 0.2 per hour, for a seizure prediction horizon of 30 and 50 min, respectively.

2.4 The Freiburg Seizure EEG Database

The Freiburg EEG database was proposed in the early 2000s as an EEG database available for download to researchers working primarily on seizure prediction. The database contains intracranial EEG recordings from 21 patients with medically intractable focal epilepsy. The recordings were acquired with a 128 channel EEG system at 256 Hz sampling rate. The database contains at least 24 hours of continuous interictal recordings for 13 patients and discontinuous inter-ictal recordings for 8 patients in addition to 50 min pre-ictal recordings from three focal and three extra-focal electrode contacts. Each patient had 2 to 5 pre-ictal recordings (average of 4.2 seizures per patient). Altogether, the database contained 582 hours of EEG data, including pre-ictal recordings of 88 seizures. Since 2012, the Freiburg database has been discontinued to be complemented and replaced by the larger EPILEPSIAE database [41] which contains data sets of annotated long-term scalp and intracranial EEG recordings from 275 patients. In this thesis, extensive analysis have been done on the Freiburg data sets mainly to assess the performance of the artifact removal algorithms for seizure predic-

tion and detection applications.

2.5 Scope of Work

To the best of our knowledge, this is the first work on mobility artifactual data acquisition in controlled and simple lab setup, as other studies used complex lab environments such as a camera mounted on a treadmill for data acquisition. As for the artifact separation technique, the well-known versatile signal processing tool ICA was adopted for artifact removal since it does not require a reference artifactual signal (unlike adaptive filters) and does not necessitate an assumption that artifacts and brain EEG signals are orthogonal (unlike PCA). Most uniquely, unlike other studies that worked with statically in-hospital recorded EEG data, this work studies the impact of mobility artifacts recorded from moving subjects as well as the effectiveness of ICA in removing these artifacts within the scope of epileptic seizure detection and prediction.

Chapter 3

Mobility EEG Data Acquisition

This chapter of the thesis describes the mobility artifactual EEG data acquisition process. The experiment involved ten subjects in a controlled lab environment with predefined speed patterns such as 120 steps/min walking EEG, 90 steps/min walking EEG, and others. The first section of this chapter presents the experimental setup followed by the procedure for mobility data acquisition and a summary of the collected information that includes EEG recordings, duration of the data files, and information about the subjects. In the second section, acquired mobility data is analyzed extensively through the comparison of patterns in acquired signals for both time and frequency domains. In addition, different statistical comparisons such as band power, total power, and zero crossing rates were established to characterize signals corresponding to different speeds of walking.

3.1 Experimental Setup

3.1.1 Headset

The DSI-24 wireless EEG headset from Wireless Sensing [52] is used as shown in 3.1 to capture EEG in real time while the user is moving in a lab environment with predetermined speeds. The headset is designed for rapid recording of continuous EEG data from the scalp. It is equipped with 21 sensors localized on the scalp based on the 10-20 international system [53]. The recorded EEG signal is sampled at 300 Hz with a resolution of 16 bits per sample.

3.1.2 Data Collection Procedure

For data collection, the headset was mounted on the participants head and the signal quality was assessed through visual inspection of EEG data and through making use of the built-in indicators for the quality of recording. In case a large impedance or disconnection between the scalp and the conductor is observed, the headset is re-positioned to

Figure 3.1: DSI-24 wearable EEG headset.

overcome any unwanted artifacts. The experimental procedure consist of six sessions with a break of two to five minutes between any two consecutive sessions. A detailed flow diagram for data collection is shown in Figure 3.2. The six sessions are divided as follows:
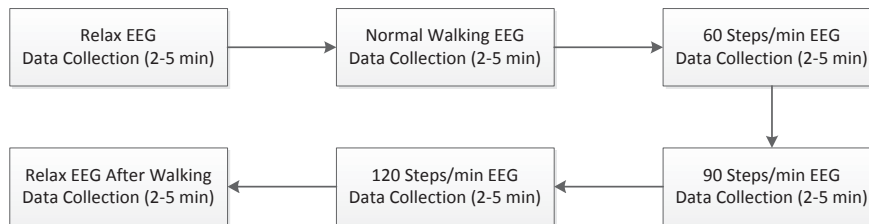
Figure 3.2: Mobility EEG data collection flow graph

1. The subject is asked to sit on a chair and relax with eyes open. EEG data is recorded for 2-5 minutes. Such data is considered clean EEG and is used for validation purposes.

2. The subject is asked to walk normally. EEG data is recorded for 2-5 minutes.

3. The subject is asked to walk with a speed of 60 steps per minute without blinking. EEG data is recorded for 2-5 minutes.

4. The subject is asked to walk with a speed of 90 steps per minute. EEG data is recorded for 2-5 minutes.

5. The subject is asked to walk with a speed of 120 steps per minute. EEG data is recorded for 2-5 minutes.

6. 7)6) Finally, the subject is asked to relax again on the chair with eyes open. EEG data is recorded for 2-5 minutes. This allows detecting any differences between EEG data for relaxed mode before and after walking.

For tracking steps per minute, a timer which produces the desired number of beep sounds per minute was used and the subject was asked to walk on the same pace as the beeps.

3.1.3 Data Collection Summary

EEG data was recorded with mobility artifacts using the aforementioned procedure from ten healthy subjects. Details for the collected data are summarized in Table 3.1. For each subject, six sets of EEG data were recorded: two of them are for relax EEG (before and after mobility) and four data sets are for normal walking with speeds of 60 steps/min, 90 steps/min, and 120 step/min. The experiment was repeated over three different days. 180 data sets were collected with a total duration of about 500 minutes. Filters were applied over the band 0.5Hz to 64Hz (with the 50Hz notch filter to eliminate power line interference).

Table 3.1: Data collection summary table

	Subject	Age	Phy. Cond.	Data Sets	Lenth(Min.)
Total	10	21-30(M)	Healthy	180	360-900

There were some difficulties while collecting EEG data using the wireless EEG headset. For example, the connections of the conductors frequently became unstable when the subject increased the walking speed (120 steps per minute or more). Another problem was that the headset Bluetooth connection was lost at times when the subject exceeded the maximum coverage range in such cases when electrodes were disconnected from the scalp or the Bluetooth connection was interrupted, a window of EEG recording containing the event was eliminated. If multiple events occurred during a single recording set and their durations added up to 5% from the total recording duration, the set was discarded.

3.2 Mobility EEG Data Analysis

The collected data was analyzed using various techniques in the time and frequency domains in order to identify the changes in EEG patterns and trends with the variations in the mobility levels.

3.2.1 Relax EEG for Different Subjects

In Figure 3.3, relax EEG data for four subjects are shown for illustration. This type of data is acquired when subjects sit on a chair in a relaxed mode. The subject was

asked to avoid excessive blinking to avoid EOG artifact. Furthermore, a band pass filter was used over the frequency band between 0.5Hz and 60Hz to avoid low and high frequency interference as well as a notch filter at 50Hz to suppress power line noise. The acquired data is sampled at 300Hz and a stretch of 5 second for relax EEG is shown in the plots. On the Y-axis, 20 electrodes are shown with their corresponding position (p for parietal, f for frontal etc.). For each electrode, scalp EEG is plotted in millivolts. The X-axis contains 1500 data points that represent time steps summing for a total of 5 seconds. The plots show a clear similarity between the recordings of different subjects for the same mobility level.
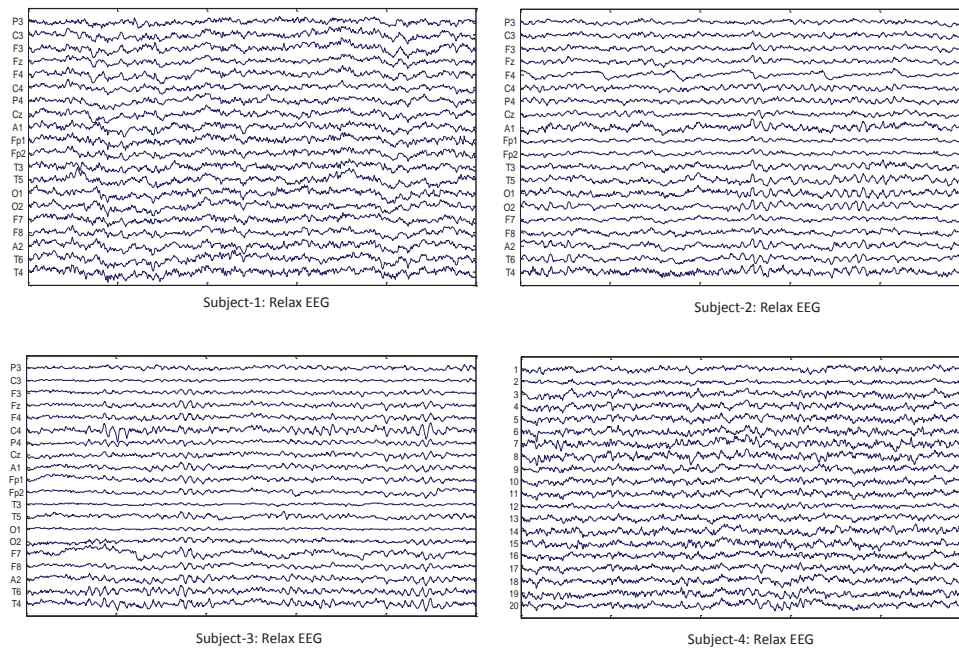
Figure 3.3: Relax EEG data comparison for different subjects

3.2.2 Normal Walking EEG for Different Subjects

Figure 3.4 represents 5 seconds EEG traces for four subjects while they were normally walking in a controlled lab setup. On the Y-axis, 20 electrodes are shown with their corresponding position (p for parietal, f for frontal etc.). For each electrode, scalp EEG is plotted in millivolts. The X-axis contains 1500 data points that represent time steps summing for a total of 5 seconds. The plots also show similarity between the recordings of different patients for the same mobility level, but they show an observable difference compared to the traces of the relax EEG. The plots also show that increasing the mobility results in increased amplitudes of the scalp voltage as well as an increased variability in the EEG signals.

17
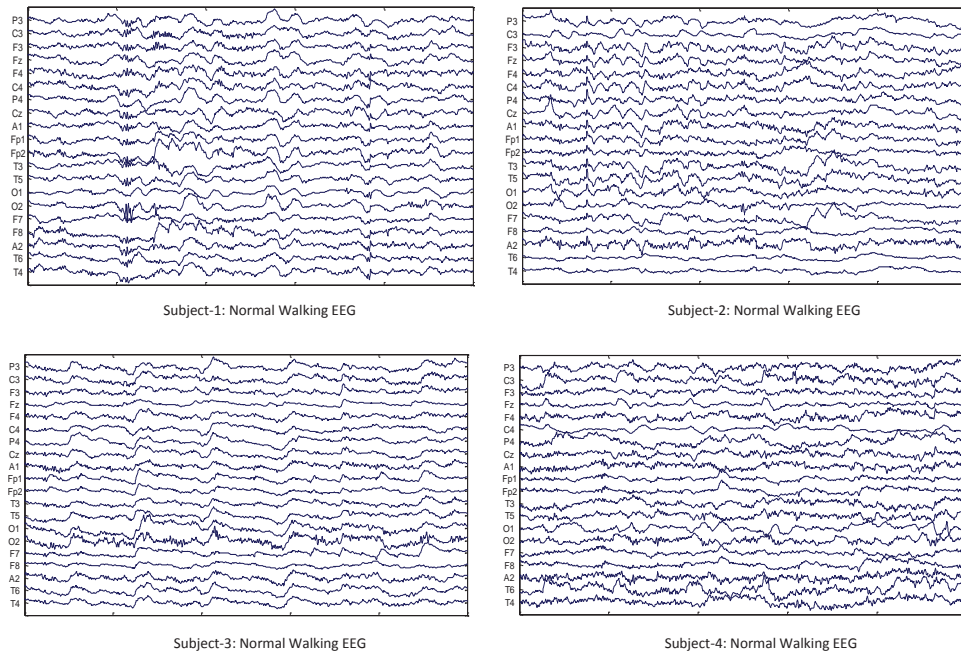
Figure 3.4: Normal walking EEG data comparison for different subjects

3.2.3 120 Steps/min walking EEG for Different Subjects

Figure 3.5 represents 5 seconds EEG traces for four subjects while they were walking with a speed of 120 steps/min in a controlled lab setup. This is the highest mobility level in terms of speed. The plots in the Figure 3.5 depicts how high peak noise appeared in every step. It is also observable that the mobility noise is being added to the brain source signal in a linear fashion. That is, the acquired data becomes noisier as the level of mobility increases. At the same time, the amplitudes of scalp voltage increase with the increase of movement speed.

3.2.4 All Mobility Data Type Comparison

Figure 3.6 shows sample EEG plots obtained using the aforementioned experimental procedure for different mobility scenarios. A clear visual difference is evident between relax time series EEG data and mobility artifactual EEG data. Relax EEG data shows low signal amplitudes and more synchronized patterns while normal walking and other predefined mobility EEG data show high signal amplitudes with less synchronization.

This difference is expected since in the relaxed case, the neurons in most of the brain regions are in the same state with low activity. On the other hand, while walking, more neurons fire and the accumulation of neural activities result in high amplitudes [8]. Moreover, these changes in neural activities alter the patterns of EEG

18
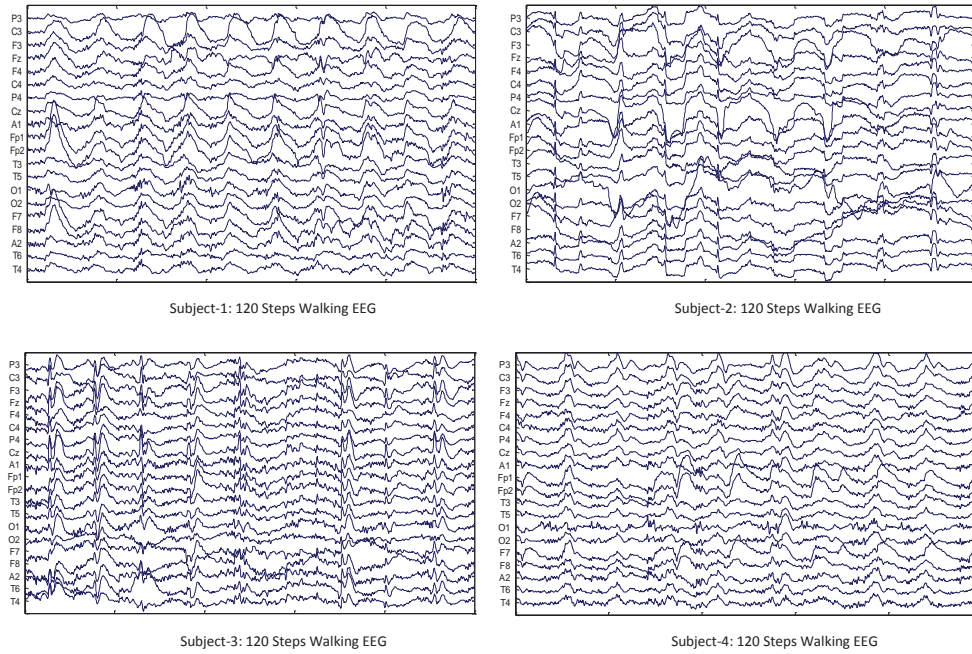
Figure 3.5: 120 steps/min walking EEG data comparison for different subjects

data what can be observed when comparing the relaxed state with the walking state. Upon comparing the relax EEG before walking and after walking, one can observe similar patterns what validates our assumption that both relaxed states are similar and correspond to the same neuronal activity of the brain. Additionally, a relationship of direct proportionality between speed and mobility noise is evident in Figure 3.6 (The higher the speed the more noisy the data becomes). This finding would help in future modeling of mobility artifacts in EEG data.

3.2.5 Power Spectrum Comparison for Different Mobility Patterns

For frequency domain comparison, the power spectrum of relax EEG opposed to different walking artifactual EEG is plotted for different subject as illustrated in Figure 3.7. From the power spectrum plots, it appears that relax EEG, both before and after walking, show a similar power spectrum while all other walking EEG show higher power over the entire frequency range. Among the different walking EEG cases, 120 steps/min shows the highest power content followed by 90 steps/min and then by normal walking EEG.

Differences in power spectrums correlate with the difference in amplitudes of the brain activity between resting modes and walking modes. The linear relation between power and speed of the mobility artifactual EEG data is also evident in Figure 3.7. The highest power is observed for 120 steps/min mobility EEG, followed by that of 90
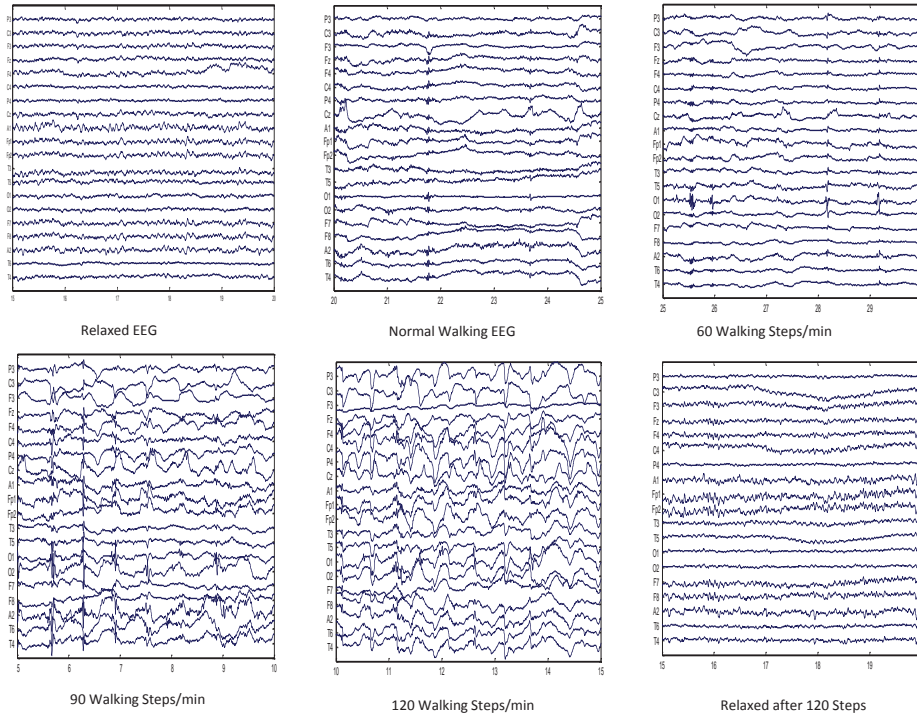
Figure 3.6: Example plot of 5 second trace of relax and different mobility EEG

steps/min EEG and then that of the normal walking EEG.

3.2.6 EEG Band Power Comparison for Different Mobility Patterns

For comparing power levels among different mobility artifactual EEG data, the power for each EEG frequency band was calculated. The bands are: Delta band (0-4Hz), Theta band (4-8Hz), Alpha band (8-16Hz), Beta band (16-32Hz) and Gamma band (32-64Hz). Detailed findings are tabulated in the subsequent section for each mobility level. Difference in power, especially in the delta band, is notable between relax and artifactual EEG. Delta waves are usually present with high amplitude and low frequency when the subject is in a sleeping state and their power increases significantly upon movement as claimed in [cite]. An almost linear increase in band power is noticed when changing state from relaxed to walking as well as when increasing the speed of walking.
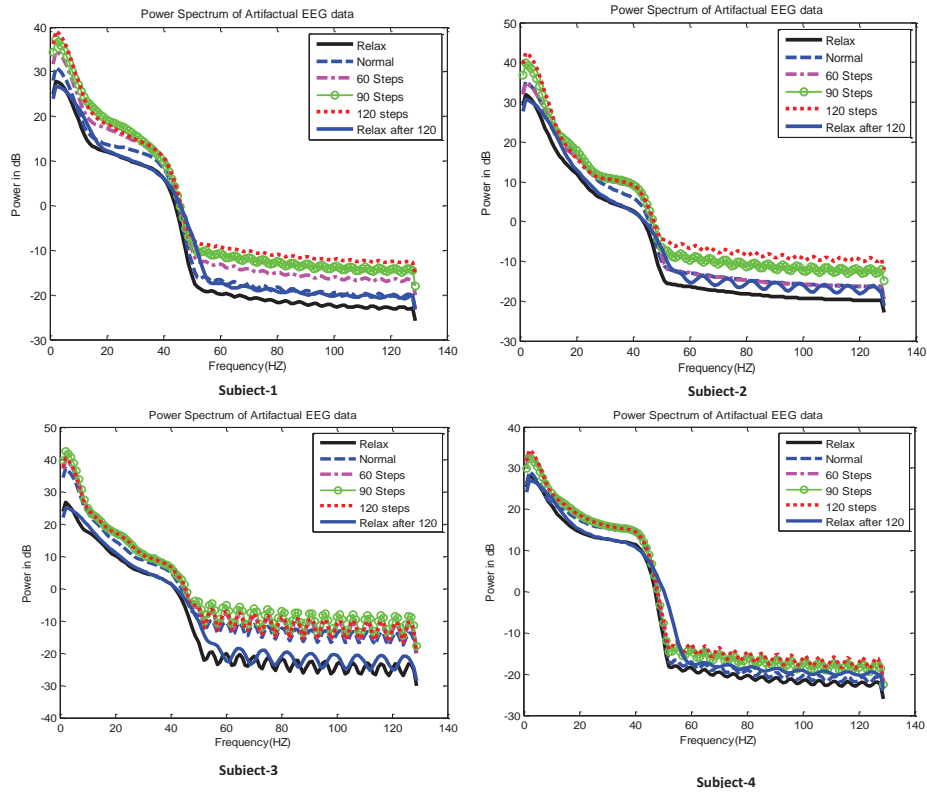
Figure 3.7: Power spectrum comparison for different mobility patterns

Band Power Comparison of Relax EEG for all Subjects

Table 3.2 represents the relative powers of different EEG bands (namely: delta, theta, alpha, beta and gamma) for relax EEG. The obtained results show that 55% of the power of relax EEG lies in delta band, 12% of the power lies in theta band, 18% of the power lies in alpha band, 8% and 3% of the power lies in beta and gamma band respectively for all ten subjects. The majority of relative powers for the delta band are between 50% and 70% while those of the gamma band always show the lowest relative power.

Band Power Comparison of Normal Walking EEG for all Subjects

For normal walking EEG, the power distribution among different bands is shown in the Table 3.3. In this case, the delta power increased to an average of 73% of the total power and it was greater than that of the relax EEG for all subjects. Notably, other band powers becomes smaller compared to those of relax EEG.

Subject	Delta Power	Theta Power	Alpha Power	Beta Power	Gamma Power
Subject-1	69.11	11.77	9.99	6.39	2.86
Subject-2	63.43	10.05	18.18	6.24	2.24
Subject-3	58.32	9.29	18.50	10.82	3.22
Subject-4	60.36	9.54	13.94	8.96	7.28
Subject-5	67.26	14.76	8.53	6.97	2.68
Subject-6	60.45	18.47	13.32	5.94	2.08
Subject-7	47.54	20.05	19.71	9.40	3.55
Subject-8	66.07	9.18	12.03	8.35	4.43
Subject-9	51.42	12.46	23.33	9.90	3.12
Subject-10	29.36	10.70	44.71	12.12	3.23

Table 3.2: Different EEG band power comparison of relax EEG for all subjects

Subject	Delta Power	Theta Power	Alpha Power	Beta Power	Gamma Power
Subject-1	72.52	13.15	6.81	4.86	2.93
Subject-2	75.24	9.09	6.62	5.51	3.64
Subject-3	71.52	11.36	8.33	5.56	3.39
Subject-4	60.79	16.16	14.06	6.78	2.31
Subject-5	70.45	8.41	11.54	6.54	3.16
Subject-6	78.24	7.84	4.93	5.05	4.08
Subject-7	73.08	10.04	8.49	5.27	3.27
Subject-8	79.65	9.05	5.12	3.58	2.67
Subject-9	76.04	11.57	6.51	3.80	2.48
Subject-10	75.99	12.29	6.97	3.19	1.70

Table 3.3: Different EEG band power comparison of normal walking EEG for all subjects

Band Power Comparison of 120 Steps/min EEG for all Subjects

The highest delta band power is reached in the 120steps/min case where it reached an average of 85% and the lowest gamma power was recorded (about 1%) as shown in Table 3.4. A key conclusion from the observations of the power distribution across frequency bands is that increasing the mobility level (i.e. the speed) results in increasing the relative power for the delta band while decreasing relative powers of all other bands.

3.2.7 Zero Crossing Rate Comparison for Different Mobility Patterns

To further evaluate the difference between relax and mobility EEG, the zero crossing rate (ZCR) test was performed for all subject cases. Details results are shown in Table 3.5, where high ZCR value is observed for relax EEG, both before and after walking, as

Subject	Delta Power	Theta Power	Alpha Power	Beta Power	Gamma Power
Subject-1	78.20	10.91	6.38	3.18	1.39
Subject-2	82.45	9.13	3.92	2.72	1.88
Subject-3	86.64	6.40	3.80	2.02	1.23
Subject-4	62.36	18.04	12.60	5.43	1.76
Subject-5	98.15	0.87	0.67	0.26	0.07
Subject-6	77.55	10.69	5.34	4.17	2.36
Subject-7	93.17	4.28	1.77	0.64	0.18
Subject-8	94.63	3.51	1.22	0.50	0.16
Subject-9	92.68	4.73	1.59	0.76	0.28
Subject-10	83.82	5.88	5.82	3.09	1.45

Table 3.4: Different EEG band power comparison of 120 steps/min EEG for all subjects

compared to different mobility EEG. It is also evident from Table 3.5 that the relationship between the ZCR value and the mobility speed is almost inversely proportional (That is, the higher the speed, the less the ZCR value becomes). It is worth noting that low zero crossing rates indicate high power while high zero crossing rates indicate low power which is consistent with the previous observations on power as shown in Figure 3.7). Moreover lower ZCR value indicate more activity of the brain neuron while high zero crossing reflects less activity [?] and it support our finding of low ZCR during walking as at this time more neurons are active. On the other hand during relax state less activity in the brain. This time we have observed an inversely proportional relationship between zero crossing rate and mobility speed that is the more speedy the EEG data is, the less ZCR rate.

Subject	Relax EEG (bf)	Relax EEG(af)	Normal Walking EEG	60 Steps/min EEG	90 Steps/min EEG	120 Steps/min EEG
Subject-1	6.74	8.20	5.63	6.20	4.55	3.86
Subject-2	7.50	7.45	4.58	4.76	2.92	2.93
Subject-3	7.91	5.12	3.08	3.37	3.17	2.81
Subject-4	8.76	6.99	5.75	6.48	5.41	4.29
Subject-5	8.67	7.18	4.51	4.66	4.44	4.84
Subject-6	7.32	6.60	3.22	1.85	2.67	1.95
Subject-7	6.06	6.48	4.78	4.64	4.43	3.32
Subject-8	5.45	4.84	3.50	1.94	1.52	2.43
Subject-9	5.94	6.23	3.07	4.25	4.20	3.07
Subject-10	7.01	7.23	4.97	5.34	4.70	3.96

Table 3.5: Zero crossing rate comparison for different mobility patterns

3.2.8   Total Power Comparison for Different Mobility Patterns

The final evaluation metric is the total power (in dB). Results for the different mobility levels are summarized in Table 3.6 for all ten subjects. It is clear that the highest total average power is recorded for the 120 steps/min EEG (1109 dB) followed by that of

the 90 steps/min EEG (600 dB) and then followed by that of normal walking EEG (300 dB). The lowest total average power is for relaxed EEG (91 dB). This stresses the linear relation between power the mobility level.

Subject	Relax EEG (bf)	Relax EEG(af)	Normal Walking EEG	60 Steps/min EEG	90 Steps/min EEG	120 Steps/min EEG
Subject-1	111.09	96.32	337.65	272.62	255.47	417.17
Subject-2	84.82	147.83	710.78	714.16	639.46	1158.21
Subject-3	36.60	40.57	181.89	154.40	625.87	543.14
Subject-4	67.46	90.75	299.12	309.06	810.89	956.49
Subject-5	172.74	158.57	232.75	204.50	177.62	304.31
Subject-6	69.50	62.18	683.07	267.25	336.59	325.48
Subject-7	102.85	69.83	269.82	188.53	971.11	3136.13
Subject-8	87.87	73.41	3626.27	315.90	1007.18	935.08
Subject-9	85.04	77.96	643.24	400.27	859.60	1797.22
Subject-10	101.17	61.70	255.95	424.75	2598.20	1524.52

Table 3.6: Total power comparison for different mobility pattern for all subjects

3.3 Summary

In summary of chapter 3, mobility artifactual EEG data was recorded in a controlled lab setup with predefined speed levels. Extensive data analysis was performed for all ten subjects in different domains (time, frequency etc.). Based on the analysis, the following was concluded. Relaxed EEG and mobility artifactual EEG are indeed different what was manifested in significant differences of their respective time and frequency domain properties as well as in their band powers and zero crossing rates. A positive correlation between the power level (mainly for the delta band) and the speed of mobility was evident for all subject cases.

Chapter 4

Mobility Artifacts Removal

This chapter proposes a procedure for removing mobility artifacts from in-lab recorded artifactual EEG data. This chapter also deals with processing of simulated noise which is added to the recorded EEG data. ICA is implemented for source separation of the pure EEG signals and the mobility artifact related components. The reconstructed noise free EEG signals are then characterized using different statistical test.

4.1 Proposed Methodology

Figure 4.1 shows a detailed scheme of the experimental setup for removing mobility artifacts. Initially, ICA is applied to EEG data corresponding to relaxed cases and to cases for different mobility levels. This results in separating data to clean and artefactual components based on visual inspection of time series and the comparison of the measures for auto correlation, power spectrum and scalp topography between components. Upon eliminating the noisy components, clean brain EEG signals are reconstructed and compared with reference relaxed EEG signals in time and frequency domains using different statistical tests such as power improvement, signal to noise ratio (SNR) improvement, etc. The bottom part of Figure 4.1 outlines the processing of simulated noise where simulated EMG artifacts are added to the recorded mobility artefactual EEG data before processing it with ICA. Similarly comparison methods are then used to assess the reconstruction capability of ICA.

4.2 Independent Component Analysis

Figure 4.1 presents an overview of the artifact removal approach which is essentially based on independent component analysis. ICA separates original signals from any set of two or more observed signal mixtures, where each signal mixture can be a linear combination of original signals [50].The success of ICA depends on some key assumptions. Mainly, source signals must be non-Gaussian and mutually statistically independent while their mixture must be Gaussian. Another key assumption is that the
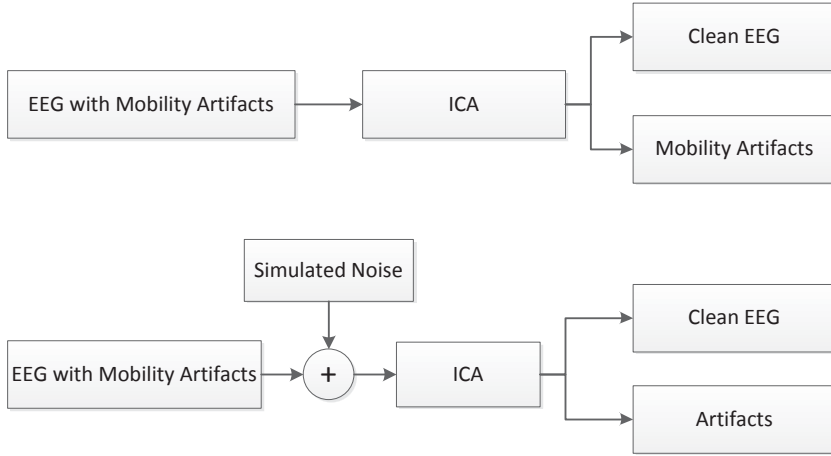
Figure 4.1: Mobility artifacts removal procedure

number of observed signals must be greater than or equal to the number of independent components of the mixture [51]. separates components based on the maximum mutual information among the sources. Equation 4.1 expresses the separated independent components in terms of the input data.

$$S = WX \tag{4.1}$$

The input to the algorithm is the collected EEG data matrix $\mathbf{X}$ of dimension $m \times N$, where m is the number of EEG electrodes and N is the total number of data points. $\mathbf{S}$ is the source activity (independent components) with a dimension of $n \times N$, where n is the number of components. The weight matrix $\mathbf{W}$ of dimension mxn is then used to express the independent components in terms of the input data.

The MATLAB toolbox, EEGLab, provides an interface for running ICA and other signal processing techniques [55].The number of components in ICA is fixed to the number of channels. The below features are used to distinguish artefactual from non-artifactual components:

- **Component Topographies:** Each artifactual component presents a unique distinguishable topography [49] which make it suitable for separation of artifactual components from brain signal.

- **Auto-correlation:** EMG artifacts are expected to have low auto-correlation [8]. For this reason, the auto-correlation have been used as a possible feature for selecting artifactual components.

- **Spectrum:**Spectrum analysis is commonly used to identify artifacts manually due to the characteristic shape corresponding to each artifact [56].

26

4.3 Signal Reconstruction Evaluation Metrics

After detecting artifactual components through the above mentioned features, noisy components are separated and clean EEG is reconstructed. The following evaluation metrics are used to validate signal regeneration as commonly used in literature [57].

1. Artifact reduction is calculated using the following equation:

$$A_{\text{Red}} = 100 \left(1 - \frac{C_{\text{ref}} - C_{\text{rec}}}{C_{\text{ref}} - C_{\text{art}}} \right) \tag{4.2}$$

C_{ref} is the auto-correlation of the reference signal, C_{art} is the cross-correlation between the artifactual and the reference signals, and C_{rec} is the cross-correlation between the reconstructed and the reference signal.

2. Signal to Noise ratio (SNR) improvement is calculated by following equation:

$$S_{\text{imp}} = 10 \log_{10} \left(\frac{V_{\text{ref}}}{V_{\text{eraf}}} \right) - 10 log10 \left(\frac{V_{\text{ref}}}{V_{\text{erbf}}} \right) \tag{4.3}$$

V_{ref} is the variance of the reference signal, V_{erbf} is the variance of the error signal before ICA, and V_{eraf} is the variance of the error signal after ICA.

3. Root Mean Square Error (RMSE) improvement is calculated using following formula:

$$R_{\text{imp}} = \sqrt{\frac{1}{N} \sum_{i=1}^{N} (x_i - \bar{x}_i)^2} - \sqrt{\frac{1}{N} \sum_{i=1}^{N} (s_i - \bar{x}_i)^2} \tag{4.4}$$

x represents the artifactual signal, $\bar{x}$ represents the econstructed signal, s represents the reference Signal, and N is the length of the EEG Data.

4. Power Spectral Density distortion improvement after ICA is found using:

$$P_{\text{imp}} = \frac{PSD_{\text{art}}}{PSD_{\text{ref}}} - \frac{PSD_{\text{rec}}}{PSD_{\text{ref}}} \tag{4.5}$$

PDS_{art} , PDS_{rec} and PDS_{ref} are the power spectral densities of the artifactual signal, the reconstructed signal, and the reference signal respectively.

5. Correlation improvement is calculated by:

$$C_{\text{imp}} = 100 \left(\frac{C_{\text{art}} - C_{\text{rec}}}{C_{\text{ref}}} \right) \qquad (4.6)$$

where C_{ref}, C_{art} and C_{rec} correspond respectively to the auto-correlations of the reference signal, the artifactual component, and the reference signal.

6. Coherence improvement

$$Ch_{\text{imp}} = 100 \left(\frac{Ch_{\text{after}} - Ch_{\text{before}}}{Ch_{\text{before}}} \right) \qquad (4.7)$$

$$Ch_{\text{after}} = \frac{G_{\text{xy}}^2}{G_{\text{xx}} * G_{\text{yy}}} \qquad (4.8)$$

G_{xy} is the cross spectral density of the reconstructed and the reference signal.

$$Ch_{\text{before}} = \frac{G_{\text{xy}}^2}{G_{\text{xx}} * G_{\text{yy}}} \qquad (4.9)$$

G_{xy} is the cross spectral density of the artifactual and the reference signal, G_{xx} is auto spectral density of the artifactual signal, and G_{yy} is the auto spectral density of the reconstructed signal.

4.4 Results: In-lab Mobility Artifacts Processing

4.4.1 Relax EEG Processing

The Figure 4.2 shows relax EEG data processing using independent component analysis. Top left plot of the Figure 4.2 represents 5 second time series EEG data of 20 channels when subject was sitting in a chair with relaxed mood. We have suggested subject to fixed eye in a fixed position to avoid ocular artifact. To avoid low and high frequency we have used band pass filter between .0.5Hz and 64Hz while recording. Top middle plot of Figure 4.2 represents reconstructed EEG after ICA implementation through selecting and separating noisy components based on time series and scal topography as shown. Reconstructed EEG is looking similar in time domain. Also the power spectrum comparison proves that relax EEG and reconstructed EEG show similar power content over the entire frequency range. This shows that ICA maintains high quality reconstruction of signals that originally contains no mobility artifacts.

Relax EEG Reconstructed EEG Power Spectrum Comparison

IC Components Component Topography
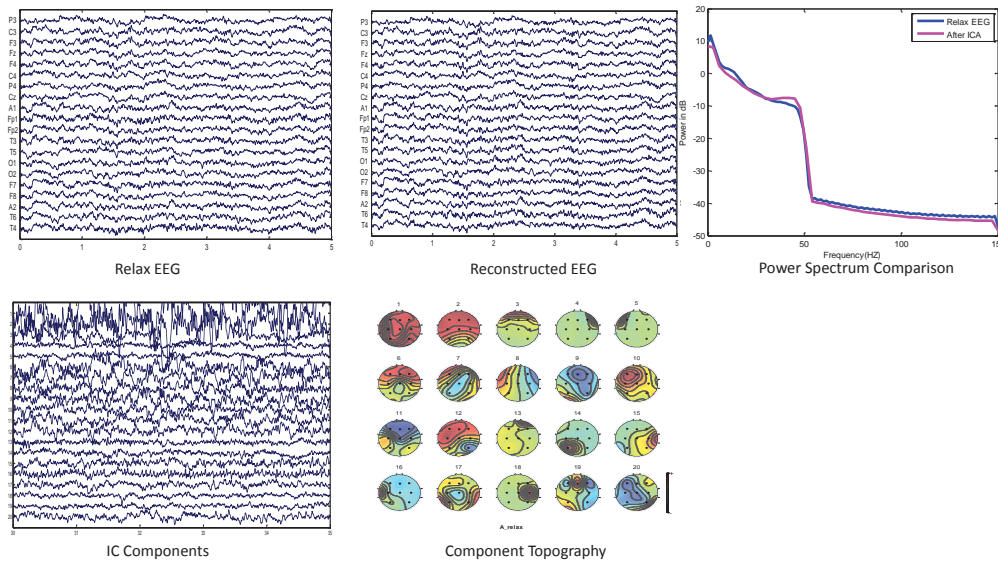
Figure 4.2: Relax EEG data processing and comparison of power spectrum

4.4.2 Normal Walking EEG Processing

Figure 4.3 illustrates the case for processing normal walking EEG data. This type of data was acquired while the subject was walking with a normal speed. Proper experimental control measures were taken to reduce and eliminate sources of artifacts other than mobility-related ones. Normal walking EEG appears noisy with clear difference compared to relax EEG. However, after ICA implementation, the reconstructed clean EEG signals, corresponding to the originally noisy normal walking EEG, appear closely comparable to relax EEG with similar power content as well.

4.4.3 120 Steps Walking EEG Processing

Figure 4.4 illustrates the case for the processing of 120 steps/min walking EEG data. The top left plot in the figure shows the time domain signals corresponding to ten channels with contaminated EEG data (The case when the subject was walking in a speed of 120 steps per minutes). The top right plot in the figure shows the scalp topography for the independents components. The middle left plot shows the time series of the ten independent components. The middle right plot shows the reconstructed EEG signals after removing the noisy components that were detected based on the scalp topography and the visual inspection of the time series for the output independent components. The bottom left plot shows the reference relaxed EEG which appears similar to the reconstructed EEG after the implementation of ICA. To validate the reconstruction capability, the power spectrum of 120 steps walking EEG is compared to the reconstructed and the relax EEG. Comparable curves are shown in the bottom right
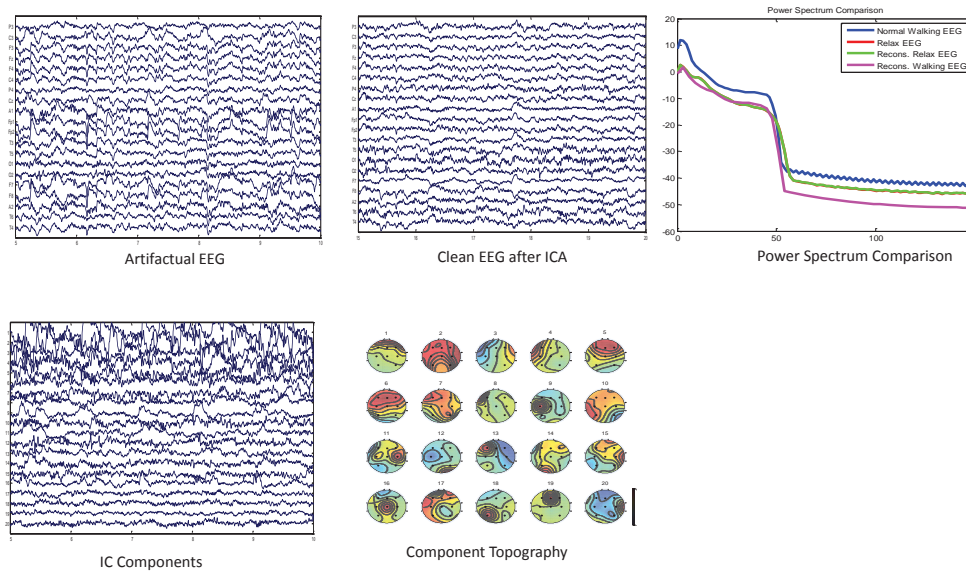
Figure 4.3: Normal walking EEG data processing and comparison of power spectrum

plot of the figure. It is notable that both relax and reconstructed EEG is showing similar power spectrums while the 120 steps walking EEG is showing higher powers over the entire frequency domain. The similarities between the spectrums of relax EEG and that of the reconstructed EEG reflects that ICA is successful and effective in separating artifactual components from brain signal.

4.5   Results: Simulated Mobility Artifacts Processing

4.5.1   Normal Walking EEG Processing

Figure 4.5 illustrates the processing of normal walking EEG data with added simulated noise using independent component analysis. The top left plot in the figure shows the time domain signals corresponding to 20 channels. These signals are for normal walking EEG. The middle top plot of the figure shows the simulated noise with the same sampling frequency and number of channels. After the addition of noise, the resulting noisy signal is shown in the top right plot of the figure. Upon processing the noisy EEG using ICA and removing the artifactual components, the reconstructed EEG signals are plotted in the bottom left plot of the figure. By visual inspection, it is clear that the reconstructed EEG is almost noise free. Also, the reconstructed noise shows similar time domain pattern to the added noise.

To further assess the quality of the reconstruction, the power spectrums of the various signals are shown in the bottom right plot. It is notable that both relax and recon-
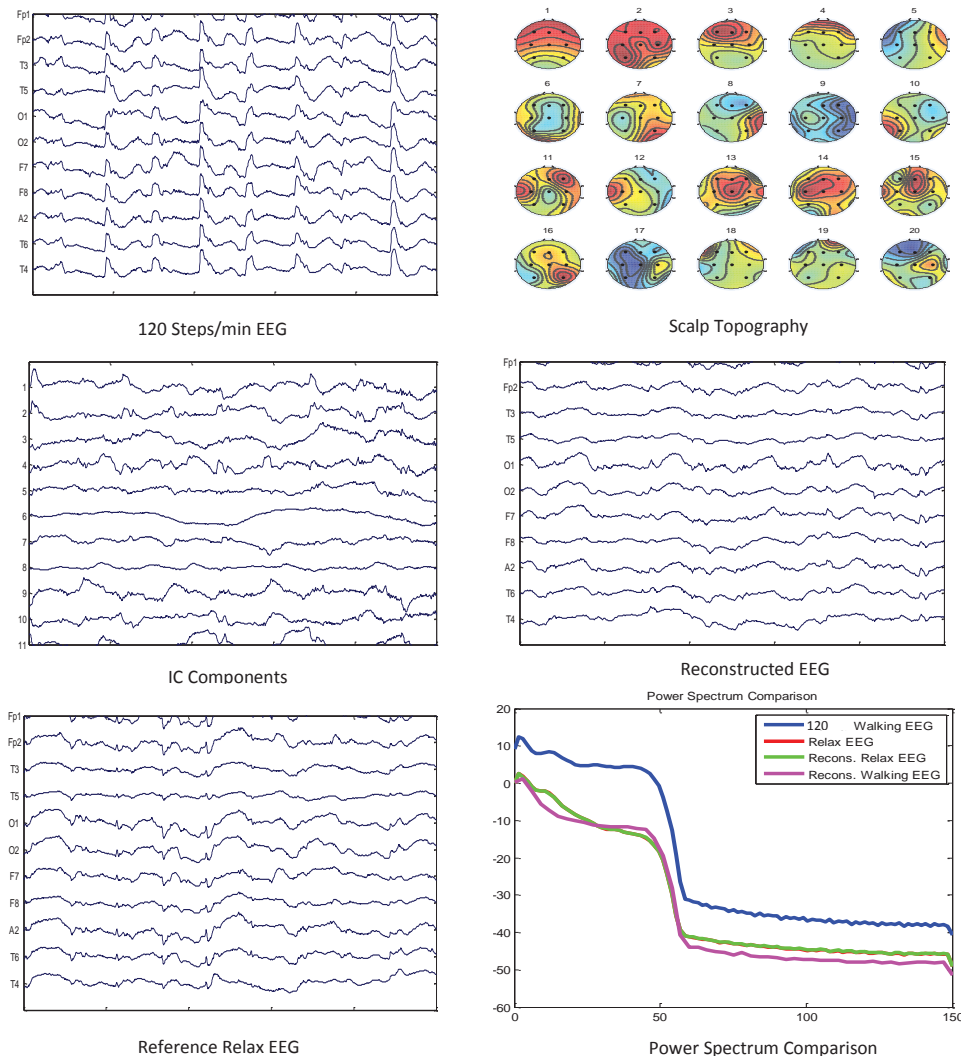
Figure 4.4: 120 walking steps/min EEG data processing and comparison of power spectrum

structed EEG is showing similar spectrums while both added noise and reconstructed noise are also showing similar temporal and spectral behavior. Again, the results prove that ICA is able to separate and remove EMG artifacts from brain EEG data.

4.5.2 60 Steps/min Walking EEG Processing

Figure 4.6 illustrates the case for processing the 60 steps/min walking EEG data after adding simulated noise. The top left plot of the figure shows the time domain signals for 20 EEG channels with mobility artifacts corresponding to the case when the subject

31
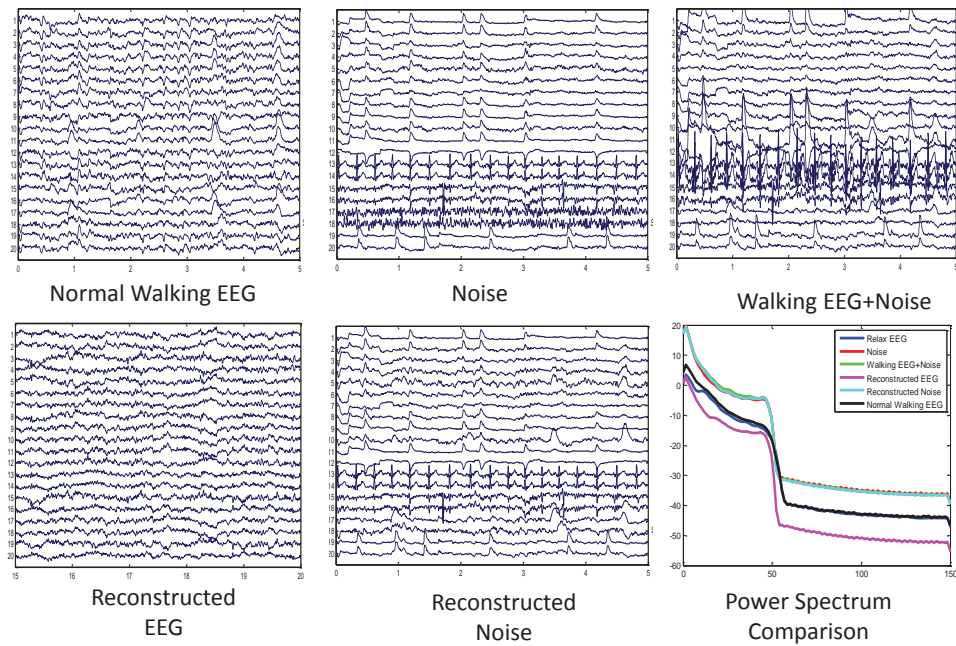
Figure 4.5: Processing of normal walking EEG data colored with simulated noise
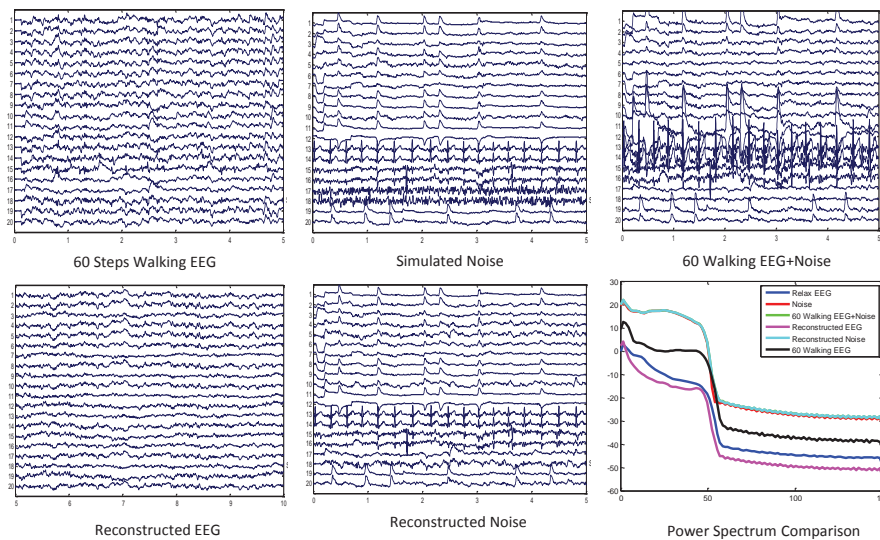
Figure 4.6: Processing of 60 steps/min walking EEG data colored with simulated noise

was walking with a speed of 60 steps per minutes. Simulated noise is added to the signals of the previous plot resulting in the noisy signals shown in the top right plot of the figure. After applying ICA, both EEG signals and simulated noise are reconstructed.

The reconstructed EEG signals appear noise-free in the time domain and show similar power spectrum to those of relax EEG as depicted in the bottom right plot of the figure. The deviation of the power spectrum for the reconstructed noise from that of the original simulated noise can be explained by the fact that the reconstructed noisy component is a mixture of the simulated noise and the noise recorded with the 60 steps EEG.

4.5.3   90 Steps/min Walking EEG Processing

Figure 4.7 illustrates the case for processing the 90 steps/min walking EEG data after adding simulated noise. The top left plot of the figure shows the time domain signals of the 20 channels with mobility artifacts corresponding to the case when the subject was walking with a speed of 90 steps per minutes. This signal is made further noisy by adding simulated noise as shown in the top right plot of the figure. After the implementation of ICA, both EEG signals and simulated noise are reconstructed. Also in this case, the reconstructed EEG seems to be noise-free and similar to the relax EEG in both time and frequency domains. The shift in the power spectrum of the reconstructed noise is also due to fact that noise here corresponds to the addition of the simulated and recorded noise.
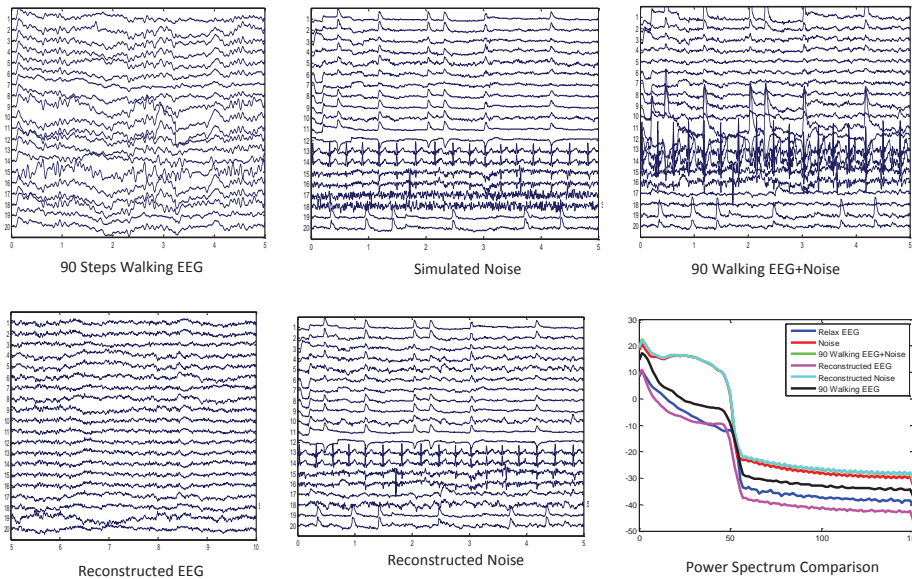
Figure 4.7: Processing of 90 steps/min walking EEG data colored with simulated noise

4.6 Statistical Validation: Artifacts Removal

4.6.1 In-lab Mobility Noise

To validate the effectiveness of ICA in eliminating recorded noise from brain EEG signals, different signal reconstruction metrics, as described in Section 4.3, are calculated and analyzed. Results are summarized in Table 4.1. On average, 10% artifact reduction, about 13 dB signal to noise ratio (SNR) improvement, and around 40 mV root mean square error improvement (RMSE) are evident for all ten subjects. The correlation and coherence improvements show around 70% and 95% respectively. These notable improvements emphasize the successful removal of mobility noise from brain EEG. They also confirm that the reconstructed signals are indeed similar in terms of correlation and coherence to the reference relax signals.

Subject	Artifact Reduction	Signal to Noise Ratio Improvement	Root Mean Square Error Improvement	Power Distortion Improvement	Correlation Improvement	Coherence Improvement
Subject-1	8.25	4.49	13.80	1.04	80.52	99.72
Subject-2	13.01	4.92	20.98	6.28	83.78	84.85
Subject-3	6.10	6.58	8.34	67.00	84.99	99.99
Subject-4	3.09	11.67	67.58	74.09	39.43	83.38
Subject-5	5.08	16.70	16.46	35.80	73.15	99.92
Subject-6	3.97	9.30	24.00	65.08	59.43	95.38
Subject-7	5.71	16.63	97.14	60.16	67.95	99.85
Subject-8	7.93	15.04	98.28	63.32	70.56	99.90
Subject-9	4.89	8.34	69.87	77.85	91.58	100.00
Subject-10	5.04	11.99	43.54	44.17	97.17	99.97

Table 4.1: Performance evaluation of ICA technique for in-lab mobility noise separation

4.6.2 Simulated Mobility Noise

Aforementioned evaluation was done for simulated noise removal. An interesting observation in the results is that after the processing of simulated noise, more significant improvements are noticeable in all of the evaluation metrics as compared to the case of in-lab recorded mobility artifacts shown in Table 4.2. The reason for this is that the amplitude of the simulated noise (160-200 V) is more significantly higher than the that of the recorded EEG (50-150 V) as compared to the recorded noise what makes simulated noise less correlated with pure EEG data and thus easier to separate and eliminate.

Subject	Artifact Reduction	Signal to Noise Ratio Improvement	Root Mean Square Error Improvement	Power Distortion Improvement	Correlation Improvement	Coherence Improvement
Subject-1	31.51	19.81	82.82	85.53	76.04	99.98
Subject-2	81.77	19.38	81.89	35.10	99.07	99.90
Subject-3	43.95	20.74	81.77	76.14	76.51	99.97
Subject-4	56.61	18.25	81.36	60.66	95.79	99.20
Subject-5	62.31	16.65	79.09	67.61	76.49	99.97
Subject-6	58.68	18.03	98.56	42.83	87.66	97.56
Subject-7	68.72	18.49	81.11	52.91	76.55	99.76
Subject-8	54.05	17.93	80.96	63.62	71.13	99.76
Subject-9	47.08	20.29	83.76	79.25	94.14	89.42
Subject-10	76.38	19.05	76.51	47.82	96.15	99.92

Table 4.2: Performance evaluation of ICA technique for simulated mobility noise separation

4.7 Regeneration Performance Test of ICA Technique

4.7.1 In-lab Mobility Noise

To test the regenerative performance of ICA, the complete 180 data sets along with another 180 simulated noisy data sets were used. The aim is to quantify the effectiveness of ICA in removing mobility artifacts and regenerating the original noise-free EEG signal. Figure 4.8 uses a boxplot to illustrate the improvement of the validation metrics used in this paper for different types of mobility EEG data after reconstruction using ICA. The plots show that the correlation and coherence improvements of both relax EEG vary between 35-80%. The improvements for all considered metrics were more significant in the cases where the subject was walking. For normal walking, a correlation improvement of 60-80% and a coherence improvement between 95% to 98% was recorded. For 60, 90 and 120 walking steps, around 50-80% correlation improvement and 95-98% coherence improvement were acheived. These improvements are expected, as we showed earlier. After ICA, the reconstructed EEG and the reference relax EEG are close both in time and in frequency domains what hints on their high correlation. Again, the spectral content of the reconstructed and the reference relax EEG are very similar what reflects the high coherence between the signals (coherence quantifies the similarity between two signal in terms of their spectral content). It can also be noted that the improvements are consistent as shown in the boxplot of Figure 4.8. For instance, the range for coherence improvement is only 3% for all subjects what shows that ICA is generating artifact-free signals with high consistency.
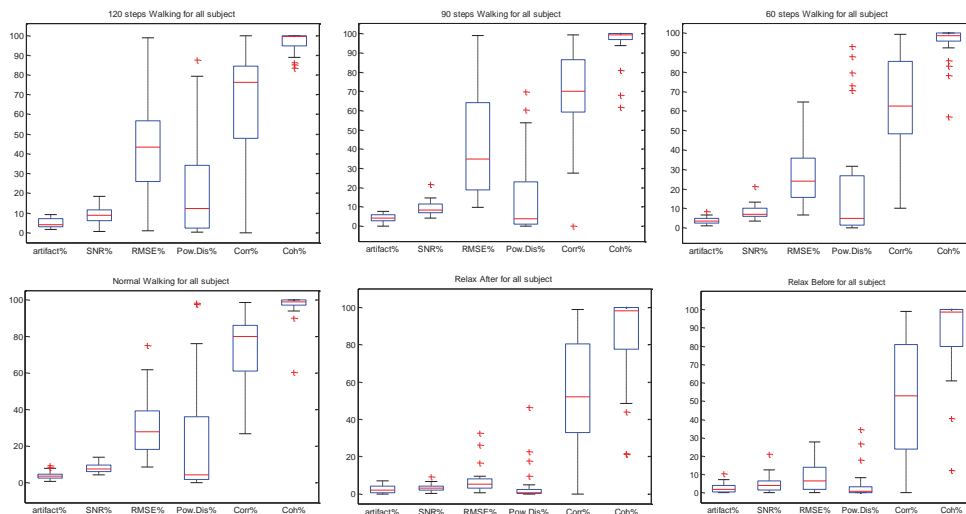
Figure 4.8: Regeneration test of ICA algorithm in processing in-lab mobility noise for all subjects
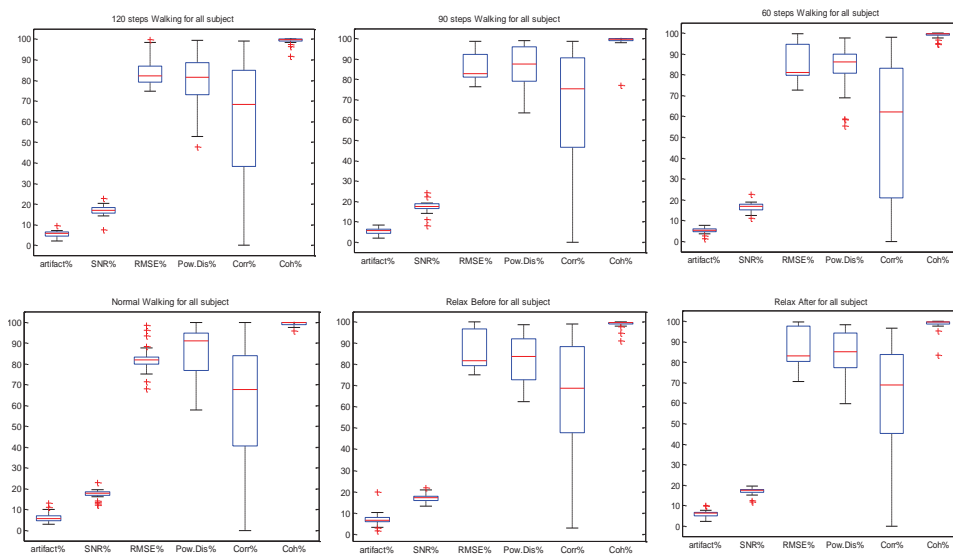
Figure 4.9: Regeneration test of ICA algorithm in processing simulated noise for all subjects

4.7.2 Simulated Mobility Noise

To further evaluate the regeneration capability of ICA, EMG noise from the Physionet EMG Database (Physionet) were added to the recorded data and the same processing

was performed. Consistent results are observed in this case except for correlation improvement which varies from 20-80% as shown in the boxplot of Figure 4.9. All other metrics such as Power distortion (75-85%) and coherence (95-97%) improvement lie within small ranges what reflects the generalized artifact-processing capability of the ICA technique. Since EMG is independent from the normal brain EEG, ICA can easily and effectively separate those simulated EMG artifacts and thus result in high correlation, power distortion and coherence improvements for the reconstructed EEG signals.

4.8   Summary

In summary, this chapter illustrates the implementation of infomax ICA algorithm from EEGLAB MATLAB toolbox for processing mobility artifactual EEG data. It also assesses ICAs capability of removing recorded mobility artifacts and simulated noise. Results in this chapter show that the reconstructed EEG signals and the separated mobility artifacts exhibit similar patterns and properties compared to their respective original sources in time and frequency domain analysis as well as in the terms of the considered statistical measures. This proves that ICA is a very effective tool for separating pure EEG data and mobility artifacts from their mixture.

Chapter 5

Impact of Mobility Artifacts on Epilepsy Detection and Prediction

The third objective of this thesis work is to conduct necessary experiments to investigate the impact of mobility artifacts on epileptic seizure prediction and detection. This chapter is designed to fulfill the aforementioned thesis goal. The chapter describes the necessary signal processing tools and machine learning algorithms for the application of epileptic seizure detection and prediction. Its first part is dedicated to test the effectiveness of ICA in eliminating mobility noise (recorded and simulated) while preserving seizure markers in the reconstructed signals. The second part deals with pre-processing, feature extraction, training and testing classification models, and finally evaluating the performance of epilepsy detection and prediction in the cases of: noise free Freiburg epileptic data, noisy epileptic data, and reconstructed epileptic data. The detailed methodology and experimental setup are described in subsequent section.

5.1   Proposed Methodology

To investigate the effect of mobility artifacts on seizure detection and prediction, mobility noise was analyzed in the case of the recorded 120 walking steps EEG and in the case of EMG simulated noise from Physionet added to the Freiburg epileptic EEG data. The proposed methodology is presented in Figure 5.1.

1. Infomax ICA is implemented on noisy Freiburg epileptic data. Noisy components are selected based on visual inspection of different time series and based on scalp topography (The noisy component selection procedure was described in Section 4.1).

2. Selected noisy components are separated from the noisy mixtures and clean epileptic data is reconstructed. The added noise is also reconstructed by sub-
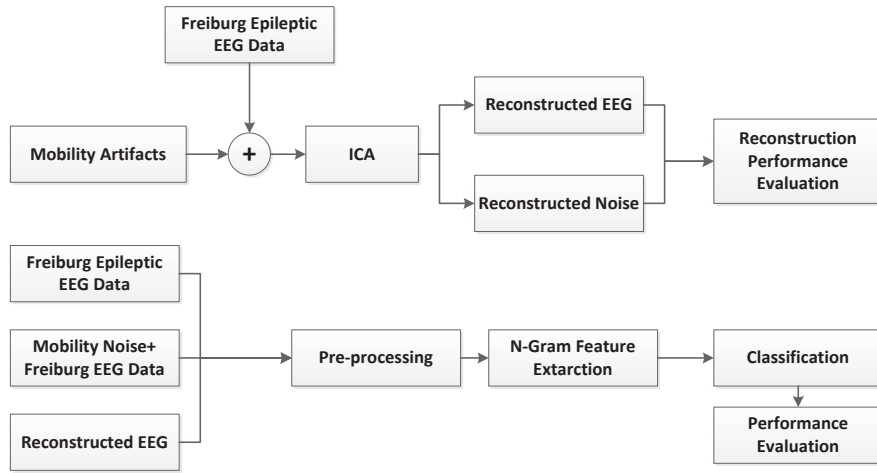
Figure 5.1: Methodology for investigation the impact of mobility artifacts on epileptic seizure application

tracting the reconstructed clean epileptic data from the noisy mixture for alter assessment.

3. Performance of ICA algorithm is evaluated in terms of the reconstruction of both epileptic data and mobility noise using different statistical signal regeneration evaluation metrics as well as time and frequency domain similarity measures. This ends the signal processing part of this chapter.

4. The Machine learning part begins with pre-processing of all data corresponding to the three type: noise-free Freiburg, noisy Freiburg (with simulated noise), and reconstructed Freiburg epileptic data after ICA. Pre-processing is necessary to avoid low and high frequencies that are insignificant in EEG diagnosis as well as to suppress power line interference. A band pass filter between 0.5Hz and 64Hz was used with a notch filter at 50Hz.

5. N-gram based feature extraction is implemented for all three data types, and it is followed by training and testing of classification models for prediction and detection. Finally, the classification capability is evaluated for all three data types using different performance evaluation metrics: accuracy, sensitivity and false alarm rate.
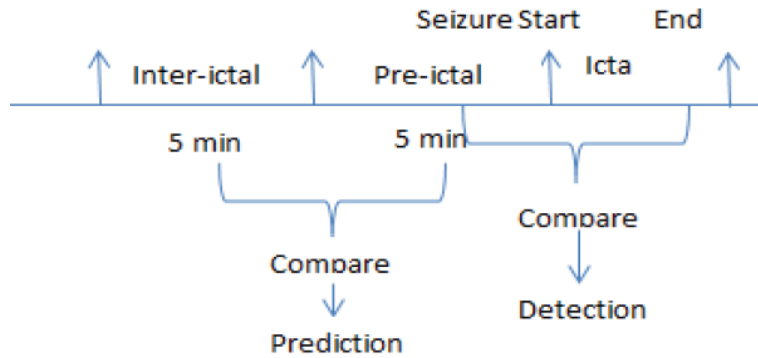
Figure 5.2: Epilepsy prediction and detection Procedure

5.2 N-gram Algorithm for Anomaly Ratio Feature Generation

An N-gram based approach was used to extract seizure distinctive features for noise free, noisy and reconstructed data. Upon training different learning models and classifying segments of EEG recordings, prediction and detection accuracies are then compared and analyzed for the three data type. For detection, learning models are trained on ictal data (from the onset of the seizure to its end) and pre-ictal (directly preceding the seizure onset). For prediction, learning models are trained on pre-ictal data and inter-ictal data (data other than pre-ictal or inter-icta). The overall scheme is depicted in Figure 5.2.

5.2.1 Overview of the N-gram Algorithm

N-gram based techniques have been previously applied in the context of EEG data analysis [35]. This work uses the N-gram approach described in [58] where sequence counts give an indicator for the variability of EEG signals. The abrupt change in the amplitude of EEG signals during seizures will reduce counts of long patterns or sequences. The gradual decrease in the pattern counts in the EEG data can be used as a marker for epileptic seizure prediction. Thus, the variability, also referred as the anomalies ratio (AR), is adopted as a distinctive feature for seizure prediction.

5.2.2 Anomaly Ratio Generation

The adopted N-gram approach relies on different parameters, namely: window size, interval length, pattern length and weight. Optimized parameters from [58] are used to run the N-gram algorithm. EEG data is analyzed in segments of length specified by the

window size. These windows of EEG data are partitioned into multiple sub-intervals whose length is determined by the interval length parameter. For every interval, time series sample values are quantized by multiplying with a conversion factor of 0.165 and dividing by a weight of 8. After quantification, the algorithm searches every interval for repeated significant patterns with a predefined pattern length. A pattern is significant if it is repeated more than a certain threshold in a particular interval (For example, if pattern [10 11 10 10 11] is repeated more than twice, it is considered as a significant pattern). Within an interval, the sample value that was not included in any of the significant patterns will be termed as un-sequenced sample. These samples are used to calculate AR for a particular interval as follows:

$$AR = \frac{\text{Count(Unsequenced Samples)}}{\text{Count(All Samples)}} \tag{5.1}$$

For feature extraction, analysis is limited to channels at which the seizure onset was clinically observed. This is due to the fact that the considered seizures are partially located on a specific region of the brain so channels that are away from the seizure onset region are not significant for prediction nor for detection.

Model Development and Classification

Ensemble learning is a technique where multiple classifiers are developed by randomly sampling the training data sets. The process of classification in ensemble learning is depicted in Figure 5.3. There are basically two approaches used in ensemble modeling namely bagging and boosting. In bagging modeling, also known as parallel modeling, ensemble models are built independently where the whole training data is divided into multiple folds using bootstrap sampling. For every fold, classifiers are trained and decisions are taken by each classifier on each test vector. The final result of classification is found by majority voting. On the other hand, boosting is a sequential approach that works by assigning high weights for miss-classified class levels. From the family of bagging ensemble modelling, the random forest classifier is used to predict seizures due to its suitable prediction and stability properties [59] as it works well for small variances in data. The random forest classifier starts by splitting the feature data into subsets for which separate decision trees are built. Each developed tree (classifier) gives a vote on any new testing feature vector. Finally the predicted class level of the tested vector is found based on majority voting or averaging. Majority voting is used for binary classification decisions while averaging is used in probabilistic classification. In the developed learning models, unbiased data sets are used with equal numbers of seizure and non-seizure feature vectors for training. For example, Patient 586 from Freiburg database has 22 recorded seizure and a total of 104 channels detected the onsets of these seizures. To develop an unbiased data set, we have generated anomaly ratios (ARs) from the ictal periods of those 104 channels. At the same time, we also extracted ARs for the same number of pre-ictal periods (with the same size as

the ictal-periods) of those channels. Thus we have a data set of 208 entries with 104 seizure cases and another 104 non-seizure cases.
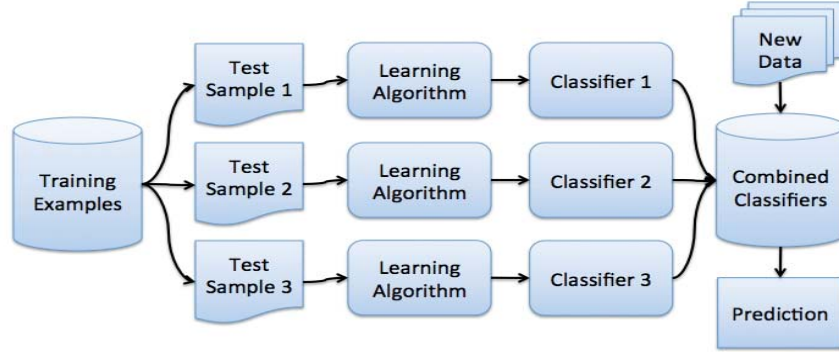
Figure 5.3: Classification model use to evaluate the impact of artifacts on epileptic seizure detection and prediction

5.2.3 Performance Evaluation

To evaluate the performance of the seizure detection and prediction algorithms, the following metrics are used:

$$\text{Accuracy} = \frac{TP + TN}{TP + FP + FN + TN} \tag{5.2}$$

$$\text{Sensitivity} = \frac{TP}{TP + FN} \tag{5.3}$$

$$\text{FalseAlarm} = \frac{FP}{FP + TN} \tag{5.4}$$

The metrics defined in (5.2)-(5.4) depend on the following variables:

1. True Positive (TP) refers to a case where an alarm is raised when a seizure actually occurred.

2. True Negative (TN) refers to a case where an alarm is not raised when a seizure did not occur.

3. False Negative (FN) refers to a case where an alarm is not raised when a seizure actually occurred.

4. False Positive (FP) refers to a case where an alarm is raised when a seizure did not occur.

5.3   Result and Discussion on Signal Reconstruction

5.3.1   Signal and Noise Regeneration Analysis

To investigate the impact of mobility artifacts on epileptic seizure prediction we have applied the same procedure we followed in Chapter 4 Section 4.1 for mobility artifacts processing.

Figure 5.4: Processing of simulated mobility artifacts from Freiburg ictal data and comparison of reconstructed signals after ICA implementation

The datasets of five patients from the Freiburg dataset were used. First, ictal data was extracted and then the mobility noise, which was originally separated from different mobility EEG data sets as discussed in Section 4.1, was added to the clean ictal data. After adding mobility noise, infomax ICA was implemented on the noisy Freiburg ictal data and artifactual components are separated and both clean ictal data and mobility noise are reconstructed. Figure 5.4 shows the separation of simulated mobility artifacts from Freiburg ictal data and the comparison of reconstructed signals after the implementation of ICA. Figure 5.5 shows separation of the in-lab recorded mobility artifacts from Freiburg ictal data and the comparison of reconstructed signals after ICA. It is clear that after adding the simulated noise, the data become more abnormal with some visible spikes. These spikes might be mistaken by learning models for seizure markers what would increase the challenge in detection and prediction. However, the reconstructed ictal signals as well as the power spectrum comparison show that ICA is able to separate the added mobility noise from Freiburg Epileptics data and thus remove misleading markers. It is notable that the reconstructed noise
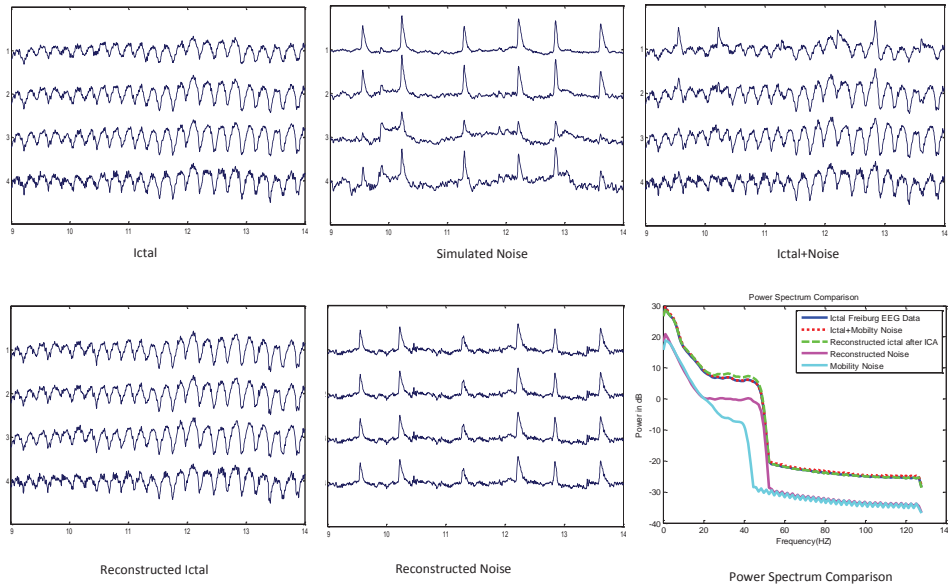
43
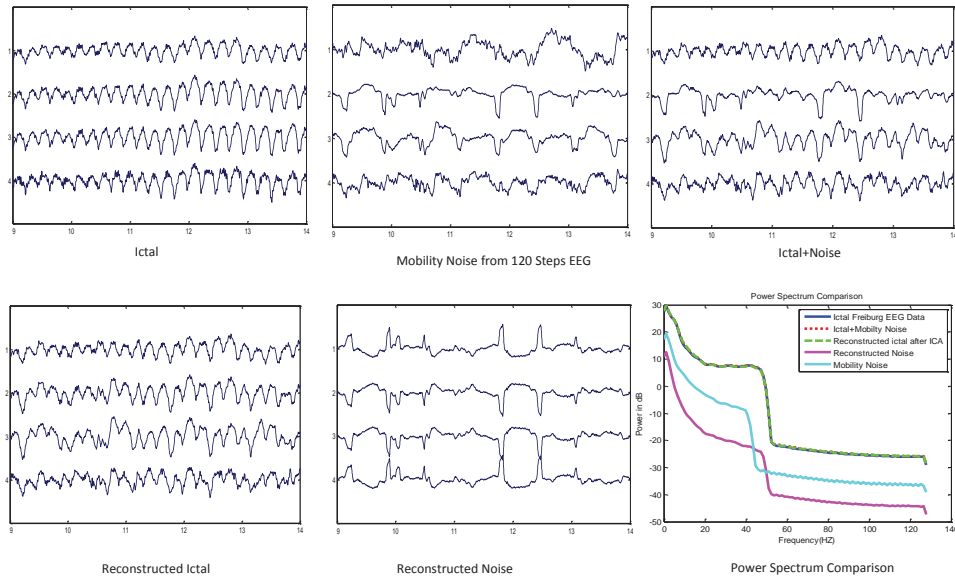
Figure 5.5: Processing of in-lab mobility artifacts from Freiburg ictal data and comparison of reconstructed signals after ICA implementation

as well as the ictal data is not perfectly similar to their respective original sources as shown in visual observation. The reason for perfect recovery is that the in-lab generated noise lacks definite patterns (unlike the simulated noise) what makes it difficult to select noisy components throughout the implementation of ICA. This was reflected in the deviation of the power spectrum as well.

5.3.2 Comparison of Noise Types

Simulated noises as well as in-lab generated noise were added to Freiburg epileptic data. Figure 5.6 we see the difference between the simulated noise and the noise extracted from the 120 steps/min recorded mobility EEG data, the latter was obtained by subtracting raw noisy data from reconstructed data. EOG and EMG noise from physionet were used as simulated noise. The two noise signals have the same size and same sampling rate (256Hz). In the simulated noise there is a clear variation from one channel to another. However, in the experimentally recorded noise, there is a pattern observed in almost all channels. This is mainly because the experimental data was recorded in a controlled lab setup with predefined speeds. This specific pattern in the 120 steps/min noise makes it easier to remove the noisy components after the implementation of ICA while at the same time, irregular patterns in the simulated noise make it difficult to identify the artifacts. Consequently, this would affect the prediction and detection capabilities shown.
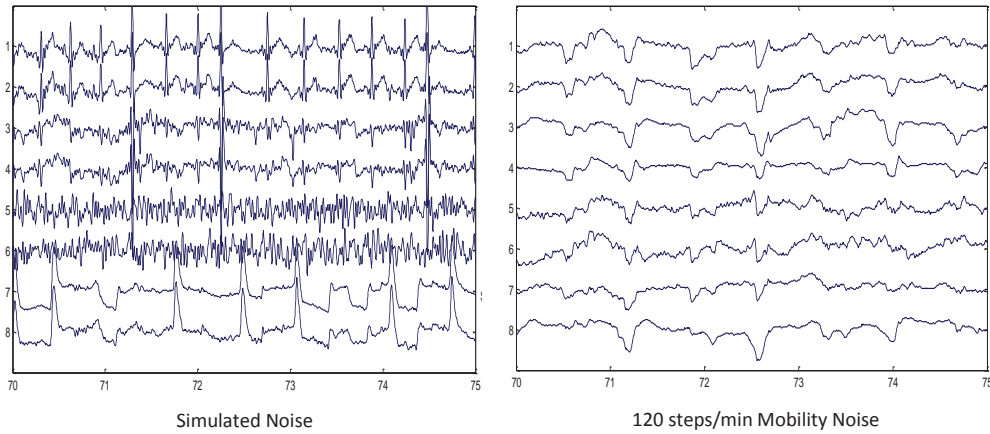
Figure 5.6: Comparison of simulated noise with in-lab mobility noise

5.3.3 Signal and Noise Similarity Test

To measure the similarity between reconstructed ictal and original ictal data as well as mobility noise and reconstructed noise we have estimated the cross correlation as shown in Figure 5.7. The cross correlation results show a strong correlation between ictal and reconstructed ictal after ICA as there is a high peak at the origin wile any shift has a relatively too low correlation. A similar correlation plot for mobility noise and reconstructed noise was obtained.

Furthermore, the similarity of the reconstructed signals is evident in both time and frequency domain as shown in Figures 5.8. In this plot, we see that both reconstructed ictal and noise show similar shape in time domain. On the other hand, ictal and reconstructed ictal show similar frequency content while reconstructed noise shows a deviation in frequency content than that of mobility noise (in right plot of Figure 5.8). One reason for this is that due to the absence of regular patterns in simulated noise, it is not possible to perfectly separate those noise components.

Finally, different statistical measures were evaluated to see the similarity between ictal and reconstructed ictal as well as between the mobility noise and the reconstructed noise. The results are summarized in Table 5.1. The table shows about 76.21% artifact improvement as well as 55.97% coherence improvement between ictal and reconstructed ictal. For the noise, the table shows around 60% artifact improvement, 99% coherence improvement, and 82% correlation improvement between mobility noise and reconstructed noise. Also, there is a substantial improvement in SNR and RMSE for both Freiburg EEG data and mobility noise. These statistical test are important in validating the previous findings recording the reconstruction capability of ICA.

45
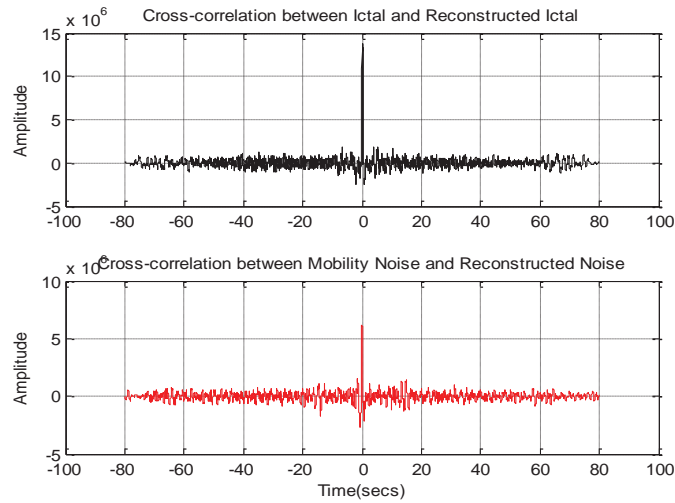
Figure 5.7: Similarity measure of ictal and reconstructed ictal, mobility noise and reconstructed noise after ICA implementation
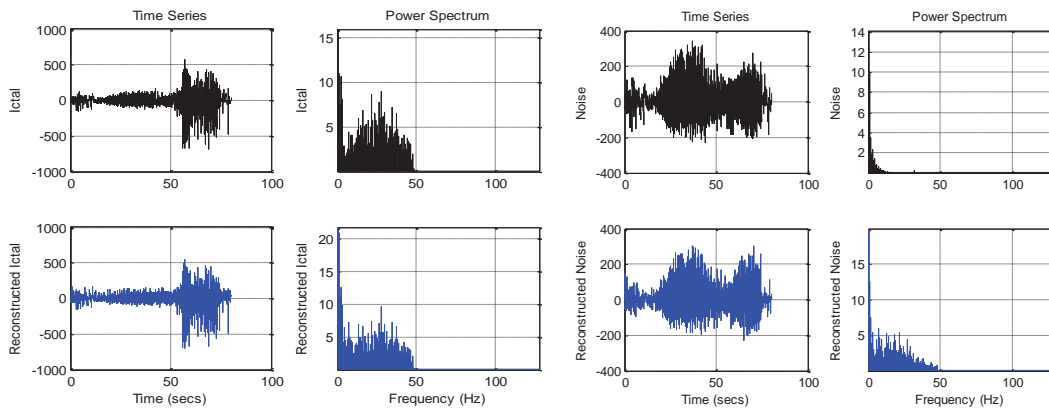
Figure 5.8: Time and frequency domain similarity measure of original and reconstructed signal after ICA implementation

5.3.4 Statistical N-Gram Analysis

Prior to applying machine learning algorithms for seizure prediction, preliminary comparison was performed for the extracted N-gram anomaly ratio (AR) values of our in-lab generated artifactual EEG data. The comparison included AR values of noisy and reconstructed data for all ten subjects. The left subplot of Figure 5.9 shows the cumulative distribution function (CDF) plot of AR values for artifactual and reconstructed EEG. The plot shows that the reconstructed EEG (dotted line) has lower AR

46

Data Type	Artifact Reduction	Signal to Noise Ratio Improvement	Root Mean Square Error Improvement	Power Distortion Improvement	Correlation Improvement	Coherence Improvement
Freiburg Epileptic EEG	76.21	11.82	18.5	1.12	1.2	55.97
Simulated Noise	60.63	10.50	44.58	22.83	37.19	99.97
120 Steps/min EEG noise	59.33	13.69	60.12	4.82	82.92	99.64

Table 5.1: Performance evaluation of ICA technique for artifact removal from Freiburg epileptic data

values compared to the noisy EEG (solid line). The right subplot of Figure 5.9 is the CDF plot for the AR values of the artifactual EEG with added simulated noise and the reconstructed EEG. In this plot, a clear difference in AR values is observed between reconstructed EEG (dotted line) noisy EEG (solid line). Reconstructed EEG shows smaller anomaly ratio values compared to noisy EEG. Another key observation is the linear increase of AR values with speed. The increase in AR values with the increase in speed is expected given the fact that the abnormal behavior of signals increase with speed what results in a lower number of significant patterns.
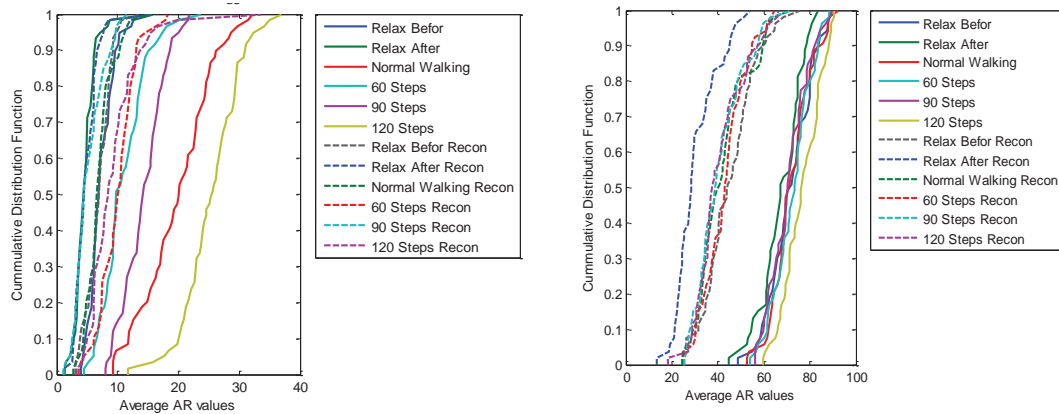
Figure 5.9: CDF plots of AR values of noisy EEG and reconstructed EEG data

AR values for ictal and pre-ictal periods of duration 2-6 min are also extracted for ten epileptic patients from Freiburg database. Figure 5.10 shows the CDF plots of the AR values for ictal (blue) and pre-ictal (red) periods of noise-free, noisy and reconstructed data. It is notable that the AR values for ictal periods are higher than those for pre-ictal periods for all three types of data sets. However, after adding mobility noise

47
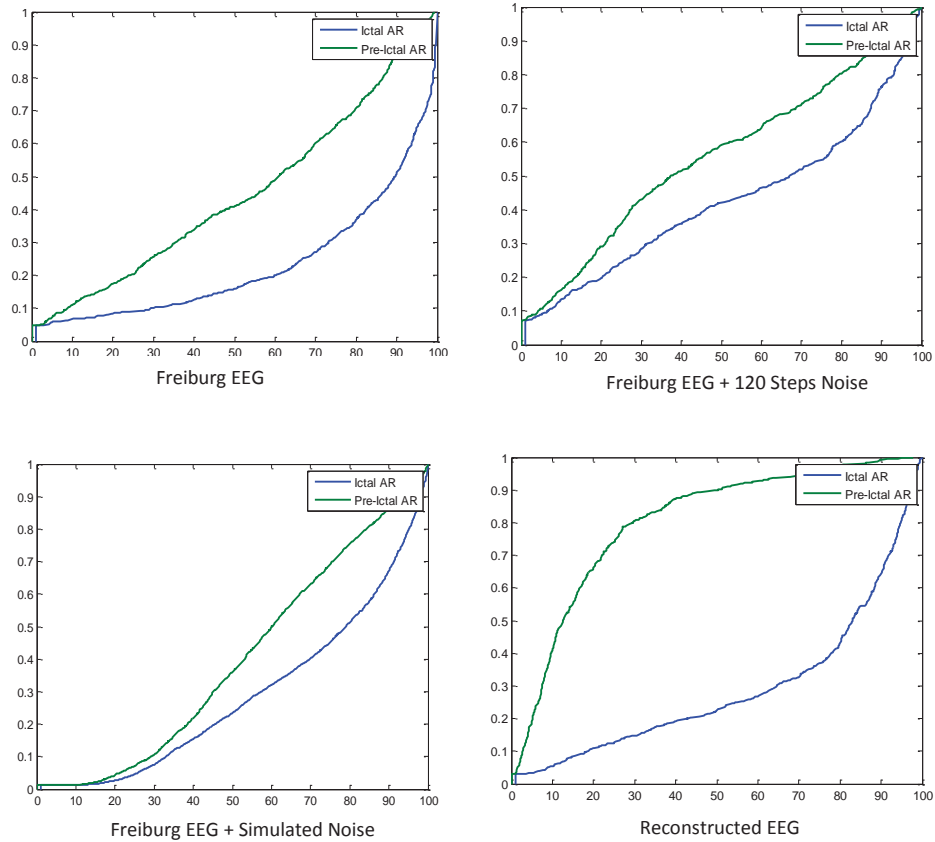
Figure 5.10: Comparison of AR values for noisy and noise free Freiburg epileptic EEG data

or in-lab generated noise, the CDF plots look similar for both ictal and pre-ictal data what imposes a challenge in the classification process. Finally, after the implementation of ICA, the difference in AR values between ictal and pre-ictal periods becomes clearer and thus easier for later classification.

5.4 Epilepsy Detection Results

To investigate the impact of mobility artifacts on epilepsy detection, N-gram features are extracted for ictal periods and pre-ictal periods from the Freiburg datasets for five epileptic patients using the same parameters (pattern length, sampling frequency, interval length, weight etc.) as used in [58]. Anomaly ratio (AR) values are calculated for noise free Freiburg EEG data, noisy Freiburg data (i.e. with added mobility noise), and reconstructed Freiburg data after ICA. The added mobility noises are either extracted from 120 steps/min walking EEG or collected from Physionet as simulated mobility

noise. Random forest classifier is then trained and tested with different validation and testing data set.

5.4.1 Hard Separation Results Analysis

To obtain an unbiased learning model, the used dataset was split into 80% for training and 20% for testing. Ten-fold cross validation was then applied on the training data to optimize models before testing. The accuracy of the optimized model was then assessed using test data what resulted highest 100% accuracy, 100% sensitivity and 0% false alarm rate is recorded for noise-free Freiburg epileptic data of patient 300 (p300) among five patients as shown in Table 5.2. After adding noise, the accuracy drops to 95.63%, the sensitivity to 92.5% and the false alarm rate increases to 1.25%. These accuracy measures improve upon ICA implementation after which accuracy increased to 97.5% and the sensitivity increased to 100%. The high accuracy and high sensitivity in the case of reconstructed Freiburg epileptic data reveal that ICA is preserving seizure markers of the ictal data while removing any misleading spikes that arise from mobility noise addition. The findings prove the applicability of ICA in the scope of seizure detection.

Training Data	Testing Data	Accuracy					Sensitivity					False Alarm				
		P1	P226	P300	P308	P586	P1	P226	P300	P308	P586	P1	P226	P300	P308	P586
Noise Free 80%	Noise Free 20 %	90	82.5	100	90	88.02	100	87.5	100	100	90.27	20	22.5	0	20	11.21
Noise Free 80%	Noisy 20%	80	82.5	94.38	73.33	86.07	83.33	85	90	71.43	87.27	22.22	20	2.5	25	11.7
Noise Free 80%	Reconstructed 20%	93	84	97.5	100	88.52	100	88	100	100	89.45	13.33	20	3.75	0	10.47

Table 5.2: Detection: hard separation results summary

5.4.2 10 Fold Cross Validation Results Analysis

Ten-fold cross validation makes use of the entire data set rather than splitting it into training and testing data. In this process, sample data is divided into 10 folds. About 90% of the sample data is picked up randomly for model development and the remaining 10% of the data is used for validation. The process is repeated 10 times so that each fold of the data is used once for testing. Detailed average results for all five epileptic patients of this approach are tabulated in Table 5.3. For noise free Freiburg data, 88.02% accuracy, 90.27% sensitivity and 11.21% false alarm rate are achieved. After adding noise, the accuracy reduces to 86.07%, the sensitivity to 87.27% and the false

alarm rate increase slightly. Upon implementing ICA, improvement is observed for all three accuracy measures: the accuracy increases to 88.52%, sensitivity to 89.45%, and the false alarm rate decreases to 10.47%. It is notable that the accuracy measures for 10-fold cross validation are lower than those of hard separation as the former results are calculated by average accuracies of all ten folds. A fold might have low accuracies if its ictal and pre-ictal AR values are similar. Nevertheless, the effectiveness of ICA for the removal of mobility noise from Freiburg data is also proven suitable for the seizure detection application as it results in standard accuracy levels.

Table 5.3: Detection: ten fold cross validation results summary

Data Type	Accuracy	Sensitivity	False Alarm
Noise Free EEG	88.02	90.27	11.21
Noisy Simulated EEG	86.07	87.27	11.7
Noisy 120 Steps EEG	87.07	88.27	11.59
Recon. Simulated EEG	88.52	89.45	10.47
Recon. 120 Steps EEG	86.07	88.27	12.12

5.4.3 Biased Results Analysis

In the biased case, the model is trained on one type of data (e.g. noise-free EEG) and tested with different types of data (noise-free, noisy, and reconstructed). In the testing phase, the test data was divided into 10 chunks and tabulated results are presented for every chunk. For noise free Freiburg data, average result of 100% accuracy, 100% sensitivity and 0% false alarm rate were recorded for all five patients as shown in Table 5.4. This high accuracy result is expected as the test data is the same as the train data. After adding mobility noise to the test data, a substantial reduction in performance is observed, sensitivity becomes 90%, accuracy becomes 94.34% and the false alarm rate increases to 1.25%. This reduction in accuracy result reveals that the added mobility noise confuses the classifier with misleading noise spikes and markers. After the implementation of ICA and the effective removal of mobility noise, the accuracy reaches 97.5% and the sensitivity reaches 98.75%. In this case as well, ICA proves capable of removing added noise while maintaining high accuracy results for seizure detection.

5.4.4 Insights Related to Epilepsy Detection

The three types of validation tests discussed earlier in Section 5.4, a clear general trend in accuracy measures is observed. Initially the detection result for noise free Freiburg is high. It falls after adding mobility noise. Results are then improved after ICA implementation. This observation stresses the applicability of ICA in seizure detection for moving patients as it removes mobility artifacts while preserving seizure markers and thus maintaining high detection accuracies.

Table 5.4: Detection: biased results summary

Train Data	Test Data	Accuracy	Sensitivity	False A.
Noise Free EEG	Noise Free EEG	100	100	0.0
Noise Free EEG	Noisy EEG	94.34	90	1.25
Noise Free EEG	Reconstructed EEG	97.5	98.75	3.75
Noisy EEG	Noise Free EEG	96.25	98.75	6.25
Noisy EEG	Noisy EEG	100	100	0.0
Noisy EEG	Reconstructed EEG	96.88	100	1.48

5.5 Epilepsy Prediction Results

While epilepsy detection is considered with correctly identifying the seizure onset by distinguishing ictal period from pre-ictal time course, epileptic seizure prediction is concerned with forecasting the onset of a seizure ahead of time without a priori knowledge of the seizure onset. In terms of difficulty, seizure prediction surely imposes greater challenges for correct classification. For prediction, the classifier must distinguish between pre-ictal periods and inter-ictal periods given the high similarity between the two as seizures do not have gradual variations preceding their onsets. Another challenge in this respect is the choice of the prediction offset; that it how early before a seizure onset shall an alarm be raised. A too long prediction offset would allow no distinction between pre-ictal and inter-ictal periods while a too short offset may hamper the patient's ability to take necessary precautions.

To investigate the impact of mobility artifacts on epilepsy prediction, N-gram features were extracted for pre-ictal and inter-ictal periods from the Freiburg datasets (datasets for patient-300 and patient-586). The same parameters as in [58] were used (pattern length- [10,8,6,4], sampling frequency-256Hz, interval length-5s, Weight-8 and Window-5 min). Anomaly ratio (AR) values are calculated for noise free Freiburg EEG data, noisy Freiburg data (i.e. with added mobility noise), and reconstructed Freiburg data after ICA. In this section, the added mobility noise is either extracted from the 90 steps/min walking EEG or collected from the simulated mobility noise. Random forest classifier is then trained and tested with different validation and testing data sets.

5.5.1 Hard Separation Results Analysis

As in the case of seizure detection, unbiased models were obtained after using 80% of the data for training and the remaining 20% for testing as shown in Table 5.5. Ten-fold cross validation is applied on the training data to develop the model and optimize it. The accuracy of the optimized model was then assessed using test data what resulted in 78.56% accuracy, 90.35% sensitivity and 35% false alarm rate for noise-free Freiburg data of patient-586. To investigate the reason for the high false alarm rate and the low

51

accuracy in prediction, preliminary analysis is performed on the AR values (features) what showed that these values are almost similar for both pre-ictal and inter-Ictal periods. Similarity in AR values confuses the classifier in distinguishing between pre-ictal and inter-ictal feature vectors. Another potential reason for the high false alarm rate in prediction could be due to hard separation and the variability of types and locations of seizures in Freiburg epileptic data [41]. This doesnt allow the learning model to be trained for all types of pre-ictal data due to hard separation. Consequently, while testing, new seizure types or locations would result in feature vectors that do not clearly correspond to pre-ictal or inter-ictal periods what leads to poor accuracy and high false alarm rate. The performance of the classifier becomes even worse after adding noise: the accuracy drops to 69.05%, the sensitivity drops to 71.43%, and the false alarm rate remains high 33.33%. However, evaluation measures for accuracy and sensitivity still improve after ICA as shown in Table 5.5: the accuracy reaches 76.19% and the sensitivity reaches 85%. The improvements achieved upon implementing ICA prove the capability of ICA to successfully remove added mobility noise from Freiburg epileptic data while maintaining standard accuracy and sensitivity results with an explainable false alarm rate.

Table 5.5: Prediction: hard separation results summary

Train Data	Test Data	Accuracy	Sensitivity	False A.
Noise Free 80%	Noise Free 20%	78.56	90.48	35
Noise Free 80%	Noisy 20%	55	75	65
Noise Free 80%	Reconstructed 20%	78.56	90.48	33.33
Noisy 80%	Noise Free 20%	69.05	71.43	33.33
Noisy 80%	Noisy 20%	70	90	28.57
Noisy 80%	Reconstructed 20%	76.19	85.71	28.56

5.5.2   10 Fold Cross Validation Results Analysis

Ten-fold cross validation makes use of the entire data set rather than splitting it into training and testing data. In this process, sample data is divided into 10 folds. About 90% of the sample data is picked up randomly for model development and the remaining 10% of the data is used for validation. The process is repeated 10 times so that each fold of the data is used once for testing. Detailed results of this approach are tabulated in Table 5.6. The obtained results for noise-free Freiburg data (patient-586) are as follows: an accuracy of 87.43%, a sensitivity of 81.73%, and a false alarm rate of 7.40% . After adding noise, the accuracy decreases to 81.19%, the sensitivity decreases to 77.91%, and the false alarm rate is doubled 15.32%. Upon the implementation of ICA, the accuracy improves to 84.64%, the sensitivity reaches 83%, and the false alarm rate is reduced to 13.90%. Improved accuracy, sensitivity, and false alarm rate results were obtained in this testing case as compared to the case of hard

separation. More importantly, the results are consistent in terms of emphasizing the applicability of ICA epileptic seizure prediction for moving patients.

Table 5.6: Prediction: ten fold cross validation results summary

Data Type	Accuracy	Sensitivity	False Alarm
Noise Free EEG	87.43	81.73	7.40
Noisy Simulated EEG	85.55	83.09	12.82
Noisy 120 Steps EEG	81.19	77.91	15.32
Recon. Simulated EEG	80.22	73.28	14.29
Recon. 120 Steps EEG	84.64	83.0	13.90

5.5.3 Biased Results Analysis

In the biased case, the learning model is trained using one data type and tested using the others as outlined in sub-section 5.4.1. For noise free Freiburg data, 100% accuracy, 100% sensitivity and 0% false alarm rate are recorded for both patient-300 and patient-586 as it is a control case. After adding mobility noise to the test data, a substantial reduction in performance is observed: the sensitivity is reduced to 86.56%, the accuracy is reduced to 86.87%, and the false alarm increases to 13.55%. After implementing ICA, the accuracy increases to 95.63%, the sensitivity increases to 97.5%, and the false alarm rate reduces to 6.25%. Therefore, this further stresses the advantage of using ICA in seizure prediction for moving patients.

Table 5.7: Prediction: biased results summary

Train Data	Test Data	Accuracy	Sensitivity	False A.
Noise Free EEG	Noise Free EEG	100	100	0.0
Noise Free EEG	Noisy EEG	86.56	86.87	13.75
Noise Free EEG	Reconstructed EEG	88.44	87.15	10
Noisy EEG	Noise Free EEG	79.68	84.38	25
Noisy EEG	Noisy EEG	100	100	0.0
Noisy EEG	Reconstructed EEG	95.63	97.5	6.25

5.5.4 Insights Related to Epilepsy Prediction

Based on the discussed three types of validation tests, an improvement in performance metrics was clearly evident upon the implementation of ICA. Initially the prediction accuracy for noise-free Freiburg is high. This is expected since in the absence of noise, AR values of pre-ictal and inter-ictal data are distinguishable. However, after adding mobility noise, AR values for both pre-ictal and inter-ictal periods appear similar (this was evident in the CDP plots of Section 5.3) what was reflected in the poor accuracy

and sensitivity results and the high false alarm rate. Upon implementing ICA and removing the artifact components, the difference in AR values reappears between pre-ictal and inter-ictal periods what improved all three prediction performance metrics. The overall findings of this section prove that ICA is capable of removing mobility noise from epileptic data while maintaining a prediction accuracy similar to that of the noise-free EEG data. This would help in developing epileptic seizure prediction systems for patients who are involved in daily life activities.

5.6   Model Validation: Student t-test

To assess the results of detection and prediction for the biased and unbiased cases, the student t-test is performed based on the hypothesis that both biased results (accuracy, sensitivity and false alarm) and unbiased results are similar. This test compares the t-value, calculated in equation 5.5, for the sample distribution (accuracy in our case) with the reference distribution table of the t-value. If the calculated t-value is greater than the t-value of the table with a certain degree of tolerance and with a certain probability (e.g. probability 5%), then we can reject our null hypothesis that two results (biased and unbiased) are different from each other with a certain confidence level (95% for the given example). The t-value is calculated using equation 5.5.

$$t = \frac{\bar{x}_1 - \bar{x}_2}{\sqrt{\frac{s_1^2}{n_1} + \frac{s_2^2}{n_2}}} \tag{5.5}$$

where $\bar{x}_1$ is mean of the accuracy for biased result, $\bar{x}_2$ is mean of the accuracy for unbiased result, s_1 is the standard deviation of accuracy result for biased case, s_2 is the standard deviation of accuracy result for unbiased case, n_1 and n_2 are number of values in biased and unbiased result respectively. $\bar{x}_1$ is the mean of the accuracies in the biased case, $\bar{x}_2$ is the mean of the accuracies in the unbiased case, s_1 is the standard deviation of accuracies in the biased case, s_2 is the standard deviation of accuracies in the unbiased case, and n_1 and n_2 correspond respectively to the number of accuracy evaluations in biased and unbiased cases. Comparing this value to values

Table 5.8: Student t-test results model validation

Model	t-value(calculated)	t-value(from table)
Hard Separation Vs Biased	1.988	1.671
Hard Separation Vs 10 Fold	2.100	1.671
10 Fold Vs Biased	2.109	1.671

in the t-distribution table [60] for a degree of freedom of 60 (sample value), the t-value is 1.671 with 90% confidence level. Since the calculated t-value is greater than table value, the null hypothesis can be rejected. Accordingly, the biased and unbiased models accuracy results are indeed different with a 90% confidence level. That is, there

is only a 10% chance for both biased and unbiased model to be same. Similarly, the t-test for the biased versus ten-fold and the ten-fold versus unbiased cases resulted in a similar conclusion. This statistical test proves that the biased results are statistically different from the unbiased results of 10-fold cross validation and hard separation.

5.7 Summary

This chapter we have investigates the impact of mobility artifacts on epileptic seizure prediction and detection. First, the signal reconstruction capability of the ICA algorithm is assessed what proved that ICA can successfully separate our added mobility noise from pure brain EEG data. This was validated using time and frequency domain characteristics as well as statistical similarity measures. After that, the effect of mobility noise on detection and prediction is analyzed extensively on Freiburg epileptic data. This shows that adding mobility noise results in a decrease of prediction and detection accuracies. Finally, the model based on reconstructed EEG signals from ICA is tested and it shows improved accuracy results. In conclusion, this chapter proves that ICA is capable of separating the in-lab recorded mobility noise as well as the simulated mobility noise from artifactual epileptic EEG data while preserving seizure markers and removing misleading spikes what consequently leads to improved accuracy results for both detection and prediction.

Chapter 6

Conclusion and Future Work

The work in this thesis was focused upon three major lines. First, physical mobility EEG data with different predefined speeds of walking was acquired in a controlled lab environment and then extensively analyzed in time and frequency domains. For this purpose, a total of 180 mobility EEG data sets with duration of 500 minutes were recorded from ten healthy subjects. Based on data analysis, the following conclusions were derived: Relaxed EEG and mobility artifactual EEG are indeed different what was manifested in significant differences of their respective time and frequency domain properties, and a positive correlation between the power level (mainly for the delta band) and the speed of mobility was evident for all subject cases.

Second, the performance of a well-known versatile signal processing technique, ICA was assessed for our in-lab recorded mobility noise and for the simulated noise. ICA was adopted as an artifact removal technique for the flexibility of its application and its superiority against other alternatives within the context of the thesis application. Filtering requires reference artifacts signal and PCA assumes that the artifacts and the source signal are orthogonal and Gaussian which does not hold in the case of mobility artifact and brain EEG signals. Since mobility artifacts and brain EEG signals are independent and nearly non-Gaussian, the required assumptions for ICA were met and thus it was the most suitable technique. Throughout the study, mobility artifactual EEG data have been processed by the infomax ICA algorithm from EEGLAB a signal processing toolbox in MATLAB. The reconstruction of brain EEG and mobility noise was then extensively analyzed using different signal regeneration evaluation metrics what helped assess the separation capability of ICA. The reconstructed EEG signal and the separated noise showed similar patterns and properties in the time and the frequency content to those of the original EEG signal and the added noise respectively. Also in terms of statistical measures, the reconstructed signals showed high correlation and coherence with the original ones. This proved the effectiveness of ICA in separating mobility artifacts from pure EEG brain activity.

Third, the challenge imposed by the mobility artifacts was considered in the context of

advanced neurological applications such as epileptic seizure prediction and detection. A thorough investigation for the impact of mobility artifacts on epileptic seizure prediction and detection was performed using both a signal processing and a data driven approach to discover any effect, if any, on prediction or detection accuracies. The effectiveness of ICA in eliminating mobility noise, both recorded and simulated, while preserving EEG signal properties and seizure markers was as well rigorously analyzed. For comparison purposes, such analysis was done for noise free Freiburg EEG data, noisy EEG data, and reconstructed epileptic data following the approach of pre-processing, feature extraction, training learning models, and classification of unlabeled EEG segments.

In term of results, a substantial artifact reduction capability was evident with an improved coherence between the original noise-free EEG signals and the reconstructed EEG signals. Improvement in SNR and RMSE was also substantial for the reconstructed signals. These statistical measures validated the previous findings that showed observable similarity between the noise-free and the reconstructed EEG signals in both time and frequency domains. For the evaluation of the epileptic seizure detection capability, three testing scenarios were investigated: biased, hard separation and ten folds division. For the three scenarios, a similar trend in accuracies was observed. The detection accuracy was initially high for noise-free data. It decreased for data contaminated mobility noise. Then it was improved after ICA implementation for the reconstructed EEG data. For epileptic seizure prediction, a similar approach was followed for evaluation. The trend in variation of accuracy was the same as that in the detection case: high for the noise-free case, lower for the noisy case, and improved for the reconstructed case. Overall, the high detection result and the standard prediction results were comparable to literature for reconstructed Freiburg epileptic EEG data. These observations led to the conclusion that ICA is capable of removing mobility noise from EEG data while preserving seizure related features and markers. Findings were unique in the scope of analyzing the effect of motion artifacts in seizure detection and prediction applications.

Future work in this area would make use of the evident correlation between mobility speed pattern and the different time, frequency and statistical features of the mobility artifactual EEG data for EEG data modeling as well as mobility noise modeling. Given that visual inspection of the noisy components was required to separate them from pure EEG data, future work can be done on the automation of the process by assigning some well-chosen data driven threshold values to separate noise from pure EEG. High detection results for reconstructed Freiburg data give hope that future epilepsy detection systems can be developed for real time monitoring. On the other hand, standard accuracy results for epileptic seizure prediction give an insight for future research in the field. Moreover, high false alarm rates for the hard separation testing case triggers curiosity to further investigate the impact of seizure types and their localization on epileptic seizure detection and prediction results. As for learning techniques, only

ensemble methods for classification were investigated, so other techniques like deep learning can also be investigated.

Appendix A

Abbreviations

AR Anomaly Ratio
BSS Blind Source Separation
CCA Canonical Correlation Analysis
CDF Cummulative Distribution Function
CT Computed Tomography
DSI Dry Sensor Interface
ECG Electrocardiogram
EEG Electroencephalography
EMG Electromyography
EOK Electrooculography
FN Flase Negative
FP Flase Positive
HMM Hidden Markov Model
ICA Independent Component Analysis
IMF Intrinsic mode function
Infomax Information Maximization
MLP Multi-channel Linear Prediction
MRI Magnetic Resonance Imaging
OA Ocular Artifacts
PCA Principle Component Analysis
PSD Power Spectral Density
RMSE Root Mean Square Error
SNR signal to noise ratio
TP True Positive
TN True Negative

Bibliography

[1] W. O. Tatum IV, *Handbook of EEG interpretation*. Demos Medical Publishing, 2014.

[2] V. Mihajlović, B. Grundlehner, R. Vullers, and J. Penders, "Wearable, wireless eeg solutions in daily life applications: what are we missing?," *IEEE journal of biomedical and health informatics*, vol. 19, no. 1, pp. 6–21, 2015.

[3] U. Braun, S. F. Muldoon, and D. S. Bassett, "On human brain networks in health and disease," *eLS*, 2015.

[4] Casson, Alexander J and Smith, Shelagh and Duncan, John S and Rodriguez-Villegas, Esther, "Wearable EEG: what is it, why is it needed and what does it entail?," pp. 5867–5870, 2008.

[5] Daly I, Nicolaou N, Nasuto S J and Warwick K , "Automated artifact removal from the electroencephalogram: a comparative study," *Clinical EEG Neuroscience*, vol. 44, pp. 291–306, 2013.

[6] I. I. Goncharova, D. J. McFarland, T. M. Vaughan, and J. R. Wolpaw, "Emg contamination of eeg: spectral and topographical characteristics," *Clinical neurophysiology*, vol. 114, no. 9, pp. 1580–1593, 2003.

[7] N. T. Anh-Dao, T. Duc-Nghia, N. Thi-Hao, T. Duc-Tan, and N. Linh-Trung, "An effective procedure for reducing eog and emg artefacts from eeg signals," in *Advanced Technologies for Communications (ATC), 2013 International Conference on*, pp. 328–332, IEEE, 2013.

[8] S. Muthukumaraswamy, "High-frequency brain activity and muscle artifacts in meg/eeg: a review and recommendations," *Frontiers in human neuroscience*, vol. 7, p. 138, 2013.

[9] K. Sweeney , T. Ward and S. McLoone, "Artifact removal in physiological signal, practices and possibilities," *IEEE Trans. Inf. Technol. Biomed.*, vol. 16, no. 3, pp. 488–500, 2012.

[10] M. N. Milanesi , N. Martini , V. Vanello , P. M. F, Santarelli and L. Landini, "Independent component analysis applied to the removal of motion artifacts from electrocardiographic signals," *Med. Biol. Eng. Comput.*, vol. 46, no. 3, pp. 251–261.

[11] K. L. Snyder, J. E. Kline, H. J. Huang, and D. P. Ferris, "Independent component analysis of gait-related movement artifact recorded using eeg electrodes during treadmill walking," *Frontiers in human neuroscience*, vol. 9, p. 639, 2015.

[12] R. Isenhart, A. Jacquin, and L. Prichep, "Method and device for removing eeg artifacts," Jan. 29 2013. US Patent 8,364,255.

[13] Croft R J and Barry R J , "Removal of ocular artifacts from the EEG: a review," *J. Clin. Neurophys.* , vol. 30, pp. 5–19, 2000.

[14] Marque C, Bisch C, Dantas R, Elayoubi S, Brosse V and Prot C, "Adaptive filtering for ECG rejection from surface EMG recordings," *J. Electromyogr. Kinesiol.: Official J. Int. Soc. Electrophysiol. Kinesiol.*, vol. 15, pp. 310–315, 2005.

[15] Sweeney K T, Ayaz H, Ward T E, Izzetoglu M, McLoone S F and Onaral B, "A methodology for validating artifact removal techniques for physiological signals," *IEEE Trans. Inf. Technol. Biomed.*, vol. 16, pp. 918–926, 2012.

[16] P. Hamilton , M. Curley , R. Aimi and C. Sae-Hau, "Comparison of methods for adaptive removal of motion artifact," *Proc. Comput. Cardiol.*, pp. 383–386, 2000.

[17] Byung Hyung Kim, Sungho Jo, "Real-time motion artifact detection and removal for ambulatory BCI," *IEEE Trans. 3rd International Winter Conference on Brain-Computer Interface (BCI)* , pp. 1–4, January 2015.

[18] Welch G and Bishop G , "An introduction to the Kalman filter," tech. rep., University of North Carolina at Chapel Hill, 2006.

[19] Jung T P, Makeig S, Humphries C, Lee T W, McKeown M J,Iragui V and Sejnowski T J , "Removing electroencephalographic artifacts by blind source separation ," *Psychophysiology*, vol. 37.

[20] James C J and Hesse C W , "Independent component analysis for biomedical signals," *Physiol. Meas.* , vol. 26, pp. 15–39, 2005.

[21] Unser M and Aldroubi A, "A review of wavelets in biomedical applications," *Proc. IEEE* , vol. 84, pp. 626–638, 1996.

[22] Huang N E, Shen Z, Long S R, Wu M C, Shih E H, Zheng Q, Tung C C and Liu H H, "The empirical mode decomposition method and the Hilbert spectrum for non stationary time series analysis," *Proc. R. Soc.* , vol. 454, pp. 903–905, 1998.

[23] T. D.-N. N.T. Anh-Dao and N. Thi-Hao, "An Effective Procedure for Reducing EOG and EMG Artefacts from EEG Signals," *International Conference on Advanced Technologies for Communications (ATC*, October 2013.

[24] Muthukumaraswamy S D , "High-frequency brain activity and muscle artifacts in MEG/EEG: a review and recommendations," *Front. Human Neurosci.* , vol. 7, pp. 138–140, 2013.

[25] J.T. Gwin, K. Gramann, S. Makeig, D.P. Ferris, "Removal of movement artifact from high-density EEG recorded during walking and running," *Journal of Neurophysiology* , vol. 130, pp. 3526–3534, 2010.

[26] Keinrath C, Zimmermann D, Scherer R , "A fully automated correction method of EOG artifacts in EEG recordings," *Clin. Neurophysiol.*, vol. 118 , pp. 98–104, 2007.

[27] J. T. Gwin, K. Gramann, S. Makeig, and D. P. Ferris, "Removal of movement artifact from high-density eeg recorded during walking and running," *Journal of neurophysiology*, vol. 103, no. 6, pp. 3526–3534, 2010.

[28] N. A. Chadwick, D. A. McMeekin, and T. Tan, "Classifying eye and head movement artifacts in eeg signals," in *Digital Ecosystems and Technologies Conference (DEST), 2011 Proceedings of the 5th IEEE International Conference on*, pp. 285–291, IEEE, 2011.

[29] A. Bertrand, V. Mihajlovic, B. Grundlehner, C. Van Hoof, and M. Moonen, "Motion artifact reduction in eeg recordings using multi-channel contact impedance measurements," in *Biomedical Circuits and Systems Conference (BioCAS), 2013 IEEE*, pp. 258–261, IEEE, 2013.

[30] B. H. Kim and S. Jo, "Real-time motion artifact detection and removal for ambulatory bci," in *Brain-Computer Interface (BCI), 2015 3rd International Winter Conference on*, pp. 1–4, IEEE, 2015.

[31] J. E. Kline, H. J. Huang, K. L. Snyder, and D. P. Ferris, "Isolating gait-related movement artifacts in electroencephalography during human walking," *Journal of neural engineering*, vol. 12, no. 4, p. 046022, 2015.

[32] W. R. LaFave *et al.*, "Search and seizure," 1978.

[33] J. Gotman, "Automatic seizure detection: improvements and evaluation," *Electroencephalography and clinical Neurophysiology*, vol. 76, no. 4, pp. 317–324, 1990.

[34] F. Mormann, R. G. Andrzejak, C. E. Elger, and K. Lehnertz, "Seizure prediction: the long and winding road," *Brain*, vol. 130, no. 2, pp. 314–333, 2006.

[35] Eftekhar A, Juffali W, El-Imad J, Constandinou TG, Toumazou C, "Ngram-derived pat-tern recognition for the detection and prediction of epileptic seizures," *PLoS ONE*, 2014.

[36] R. S. Fisher, W. v. E. Boas, W. Blume, C. Elger, P. Genton, P. Lee, and J. Engel, "Epileptic seizures and epilepsy: definitions proposed by the international league against epilepsy (ilae) and the international bureau for epilepsy (ibe)," *Epilepsia*, vol. 46, no. 4, pp. 470–472, 2005.

[37] Bandarabadi M, Teixeira CA, Rasekhi J, Dourado A, "Epileptic seizure prediction using relative spectral power features," *Clin Neurophysiol.*, vol. 126, no. 2, pp. 237–248, 2015.

[38] Cook MJ, O'Brien TJ, Berkovic SF, Murphy M, Morokoff A, Fabinyi G, "Prediction of seizure likelihood with a long-term, implanted seizure advisory systemin patients with drug-resistant epilepsy: a first-in-man study," *Lancet Neurol.*, vol. 12, pp. 563–571, 2013.

[39] K. M. D. F. Schindler K, Wiest R, "EEG analysis with simulated neuronal cell models helps to detect pre-seizure changes," *Clin. Neurophysiol.*, vol. 113, pp. 604–614, 2002.

[40] Aarabi A, He B., "Seizure prediction in hippocampal and neocortical epilepsy using a model based approach," *Clin Neurophysiol.*, vol. 125, pp. 930–940, 2014.

[41] M, Feldwisch-Drentrup H, Teixeira CA, Witon A, Schelter B, Timmer J, "EPILEPSIAE European epilepsy database," *Comput Methods Programs Biomed.*, vol. 106, pp. :127–138, 2012.

[42] P. L. Nunez and R. Srinivasan, *Electric fields of the brain: the neurophysics of EEG*. Oxford University Press, USA, 2006.

[43] A. S. Gevins, W. Du, and H. Leong, "Adaptive interference canceler for eeg movement and eye artifacts," May 7 1996. US Patent 5,513,649.

[44] X. Miao, H. Huang, X. Hu, D. Li, Y. Yu, and Y. Ao, "The characteristics of eeg power spectra changes after acl rupture," *PloS one*, vol. 12, no. 2, p. e0170455, 2017.

[45] R. Sameni, M. Shamsollahi, and C. Jutten, "Model-based bayesian filtering of cardiac contaminants from biomedical recordings," *Physiological Measurement*, vol. 29, no. 5, p. 595, 2008.

[46] G. Chabriel, M. Kleinsteuber, E. Moreau, H. Shen, P. Tichavsky, and A. Yeredor, "Joint matrices decompositions and blind source separation: A survey of methods, identification, and applications," *IEEE Signal Processing Magazine*, vol. 31, no. 3, pp. 34–43, 2014.

[47] T.-P. Jung, C. Humphries, T.-W. Lee, S. Makeig, M. J. McKeown, V. Iragui, and T. J. Sejnowski, "Removing electroencephalographic artifacts: comparison between ica and pca," in *Neural Networks for Signal Processing VIII, 1998. Proceedings of the 1998 IEEE Signal Processing Society Workshop*, pp. 63–72, IEEE, 1998.

[48] A. Delorme, T. Sejnowski, and S. Makeig, "Enhanced detection of artifacts in eeg data using higher-order statistics and independent component analysis," *Neuroimage*, vol. 34, no. 4, pp. 1443–1449, 2007.

[49] S. Olbrich, J. Jödicke, C. Sander, H. Himmerich, and U. Hegerl, "Ica-based muscle artefact correction of eeg data: What is muscle and what is brain?: Comment on mcmenamin et al.," *Neuroimage*, vol. 54, no. 1, pp. 1–3, 2011.

[50] J. V. Stone, *Independent component analysis*. Wiley Online Library.

[51] M. J. McKeown, T. J. Sejnowski, *et al.*, "Independent component analysis of fmri data: examining the assumptions," *Human brain mapping*, vol. 6, no. 5-6, pp. 368–372, 1998.

[52] A. Pantelopoulos and N. G. Bourbakis, "A survey on wearable sensor-based systems for health monitoring and prognosis," *IEEE Transactions on Systems, Man, and Cybernetics, Part C (Applications and Reviews)*, vol. 40, no. 1, pp. 1–12, 2010.

[53] R. W. Homan, J. Herman, and P. Purdy, "Cerebral location of international 10–20 system electrode placement," *Electroencephalography and clinical neurophysiology*, vol. 66, no. 4, pp. 376–382, 1987.

[54] M. Milanesi, N. Martini, N. Vanello, V. Positano, M. F. Santarelli, and L. Landini, "Independent component analysis applied to the removal of motion artifacts from electrocardiographic signals," *Medical & biological engineering & computing*, vol. 46, no. 3, pp. 251–261, 2008.

[55] A. Delorme and S. Makeig, "Eeglab: an open source toolbox for analysis of single-trial eeg dynamics including independent component analysis," *Journal of neuroscience methods*, vol. 134, no. 1, pp. 9–21, 2004.

[56] P. Hamilton, M. Curley, R. Aimi, and C. Sae-Hau, "Comparison of methods for adaptive removal of motion artifact," in *Computers in Cardiology 2000*, pp. 383–386, IEEE, 2000.

[57] M. K. Islam, A. Rastegarnia, and Z. Yang, "A wavelet-based artifact reduction from scalp eeg for epileptic seizure detection," *IEEE journal of biomedical and health informatics*, vol. 20, no. 5, pp. 1321–1332, 2016.

[58] H. Alawieh, H. Hammoud, M. Haidar, M. H. Nassralla, A. M. El-Hajj, and Z. Dawy, "Patient-aware adaptive ngram-based algorithm for epileptic seizure prediction using eeg signals," in *e-Health Networking, Applications and Services (Healthcom), 2016 IEEE 18th International Conference on*, pp. 1–6, IEEE, 2016.

[59] C. Donos, M. Dümpelmann, and A. Schulze-Bonhage, "Early seizure detection algorithm based on intracranial eeg and random forest classification," *International journal of neural systems*, vol. 25, no. 05, p. 1550023, 2015.

[60] "https://www.medcalc.org/manual/t-distribution.php,"